WINDS OVER TROUBLED WATERS: TEMPORAL CHANGES IN THE ONSET AND INTENSITY OF COASTAL ALONGSHORE WINDS IN THE PACIFIC NORTHWEST

by

Brian Bylhouwer
B.Sc. (Physics) University of Prince Edward Island

RESEARCH PROJECT SUBMITTED IN PARTIAL FULFILLMENT
OF
THE REQUIREMENTS FOR THE DEGREE OF

MASTER OF RESOURCE AND ENVIRONMENTAL MANAGEMENT
(MRM)

In the
School of Resource and Environmental Management

SIMON FRASER UNIVERSITY

Summer 2012

APPROVAL

Name:	**Brian Bylhouwer, B.Sc.**
Degree:	**Master of Resource Management**
Title of Thesis:	**Winds Over Troubled Waters: Temporal Changes in the Onset and Intensity of Coastal Alongshore Winds in the Pacific Northwest**
Project No.:	**556**

Examining Committee:

Chair: **Carolyn Duckham, B.Sc.**

_____

Dr. Karen E. Kohfeld
Senior Supervisor
Assistant Professor
School of Resource and Environmental Management
Simon Fraser University

_____

Dr. Debby Ianson
Supervisor
Adjunct Professor
School of Resource and Environmental Management
Simon Fraser University

Date Defended/Approved: _____

ABSTRACT

The timing, duration, and intensity of wind-driven upwelling and downwelling along the north Eastern Pacific coast play an integral role in coastal circulation and basin-wide ecosystem composition. It has been suggested that global warming will cause changes in these winds. Here we develop objective criteria to determine the onset, duration and intensity of upwelling and downwelling seasons due to local wind forcing. We use these criteria to examine and better characterize temporal trends in wind-driven coastal currents by allowing a flexible onset to each season, and relate them to global warming and large-scale climate oscillations in the coastal ocean between northern California and Vancouver Island (39° and 51°N). We find an exceptionally variable onset of upwelling at all locations. No significant trends in the timing and duration were found. Positive phases of the Pacific Decadal Oscillation are correlated to later and shorter upwelling seasons, but not necessarily weaker upwelling. Warm phases of the El Niño Southern Oscillation are correlated with an earlier onset of summer upwelling, and with more intense downwelling throughout the study area. Our analysis identifies strong interannual to interdecadal variability, and the importance of time series length when isolating physical temporal trends influenced by large-scale oscillatory behaviour of the climate.

Keywords: Alongshore winds; Time series experiments; Upwelling; Global Change; Interannual variability; Eastern North Pacific.

DEDICATION

This work, and all of its trials and tribulations, and its ultimate culmination, is, in a small, humble way, dedicated to God, from whom all good things come.

ACKNOWLEDGEMENTS

Thank you to the many who have inspired, encouraged, pushed, and supported me through this process, especially:

- Karen Kohfeld, for opening the door to a whole new world of Environmental Management while keeping me firmly planted in the physical sciences, and for having the perfect blend of challenging ideas and inspiring independent thought;
- Debby Ianson, for being a second-to-none research navigator, and for always being up for a coffee to talk things over;
- Tommy Rodengen, Ben Cross, Liz Sutton, Christie Spry, Carolyn Duckham, and Celeste Barlow, for your attentive ears and insightful comments during each stage of the research process;
- To the 2009 REM cohort, for changing the way I think in many ways, and confirming the way I already thought in others;
- Lastly, but foremost, to my two loves, Amy and our daughter Elizabeth Bylhouwer: for following me from the Atlantic to the Pacific, and back again; for your patience; and for reminding me every day about what is most important in life.

Thanks also to the National Science and Engineering Research Council, the Climate Change Impacts Research Consortium, Simon Fraser University, and the Department of Fisheries and Ocean Canada for supporting this work.

TABLE OF CONTENTS

LIST OF FIGURES

LIST OF TABLES

1: INTRODUCTION

The California Current System (CCS) from Vancouver Island to northern California has been well studied due to its high levels of primary productivity and availability of commercially viable fisheries such as anchovies, sardines, shrimp, mackerel, hake, sablefish and salmon [Ware and Thomson, 1991; Thomson and Ware, 1996; Mackas, 2006; Hickey and Banas, 2008; Chavez et al., 2009]. Productivity in the CCS is primarily driven by nutrients delivered by upwelling; the timing and intensity of upwelling can therefore heavily influence the composition and vitality of biota at all life stages [Ware and Thomson, 1991, 2005; Mackas et al., 2001; Barth et al., 2007].

Both upwelling and downwelling processes in the CCS also influence the regional carbon cycle. Upwelling occurs primarily in the summer season when equatorward winds cause offshore advection of surface coastal water, resulting in the episodic shoaling of cold, carbon- and nutrient-rich, and oxygen-poor intermediate depth (~100 m) water at the coast [Pond and Pickard, 1981;Smith et al., 1994; Park et al., 2008]. CO2 outgassing can occur immediately following periods of upwelling, but the subsequent primary production turns surface waters into a carbon sink [Ianson and Allen, 2002; Hales et al., 2005]. During the winter season, poleward winds cause coastal downwelling in the northern portion of the CCS, which temporarily depresses the pycnocline [Smith et al., 1994] and translocates waters potentially rich in carbon off the shelf into the adjacent

subsurface ocean basin [Hales et al., 2005]. The net annual carbon budget is confounded by the intensity of upwelling relative to downwelling, as well as the bathymetric characteristics of the coastal shelf [Ianson et al., 2009].

Studies have suggested that climate change could influence the intensity of wind-driven upwelling and downwelling winds, which is expected to have a substantial impact on future productivity and carbon cycling [Auad et al., 2006; Merryfield et al., 2009; Bakun et al., 2010]. Global warming has been linked to enhanced, upwelling-favourable, alongshore winds for major global eastern boundary currents [Bakun, 1990]. Time series analyses of the CCS have confirmed this relationship south of 40 degrees latitude between 1945 and 2008. [Hsieh et al., 1995; Schwing and Mendelssohn, 1997; Garcia-Reyes and Largier, 2010]. A meta-analysis of General Circulation Model (GCM) forecasts as well as Regional Circulation Model (RCM) analyses have also shown increasing upwelling winds along the entire CCS from 1990 to 2100. However, no statistically significant trend in winter downwelling has been observed at more northern latitudes [Snyder et al., 2003; Auad et al., 2006; Merryfield et al., 2009].

Climate-induced changes to the onset of upwelling and downwelling seasons could also have important implications for marine ecosystems, but these changes have been studied less systematically. For example, the onset of the upwelling season has been found to primarily determine the biological composition of ecosystems in the north Eastern Pacific [Ware and Thomson, 2005; Barth et al., 2007]. Enhanced winter downwelling has also been associated with lower primary production during the spring transition on the west coast of

Vancouver Island [Ianson and Allen, 2002; Tortell et al., submitted]. Shifts in the onset of summer upwelling or winter downwelling could cause detrimental mismatches between nutrient delivery and subsequent productivity and life cycle stages of several pelagic fish species, independent of any change in upwelling or downwelling magnitude [Beaugrand et al., 2003; Edwards et al., 2004; Bakun et al., 2010]. Multiregional shifts in oceanographic conditions have been proposed as a potential cause of for the region-wide decline in sockeye salmon since 1990 in the Pacific Northwest [Peterman and Dorner, 2012]. Most studies of temporal trends in coastal winds along the CCS assume the start and end dates of oceanographic summer and winter seasons are stationary in time, despite evidence to the contrary [e.g. Thomson and Ware, 1996]. Furthermore, few studies examine the influence of large-scale climate oscillations such as the El-Niño Southern Oscillation (ENSO), the Pacific Decadal Oscillation (PDO) or the North Pacific Gyre Oscillation (NPGO), which could also account for temporal trends in historical analyses [Garcia-Reyes and Largier, 2010].

The goal of this research is to evaluate temporal changes in the seasonal onset, duration, and intensity of upwelling and downwelling seasons in the CCS for 1948-2010. Using time series datasets of wind speeds from reanalysis as well as lighthouse and buoy data, we first develop and test simple and objective criteria to demarcate the winter, summer, and two transition seasons. Using our established criteria, we examine temporal changes in the onset and duration of each season, from Vancouver Island to northern California. Finally, we compare these data with well-established patterns of climate oscillatory behaviour.

2: METHODS

2.1 Study Area and Data Sources

Our study area encompasses the coastal region between northern Vancouver Island (50.91° N) and San Francisco (37.14° N) out to the continental shelf break (Figure 1). Three-hourly wind data were retrieved from North American Regional Reanalysis (NARR [Messinger, 2005]) and National Centre for Environmental Prediction (NCEP; [Kalney et al., 1996]) interpolated models (Figure 1), and hourly wind data were collected from Environment Canada (EC) and National Oceanographic and Atmospheric Administration (NOAA) buoy and lighthouse stations (Figure 1). All data were standardized to 10-metre height [Zoumakis, 1993], and vector-averaged into daily values of wind speed and direction. To control for gaps in the data, daily observational data were omitted if less than 7 hourly wind measurements were recorded. Temporal coverage of observational data was poor even without this threshold, particularly with buoy stations. Temporal gaps ranged from a single day to over 1300 days (Figure 1 in supplementary material). The number of individual gaps range from 19 to 175 days per record and the total number of days missing for an individual location range from 158 to 3860 (Table 1 in Appendix A). Observational data were therefore used only to ground-truth NARR and NCEP data for this study.

The NARR data set contains meteorological variables constructed by interpolating observations of temperature, wind speed, and pressure onto a

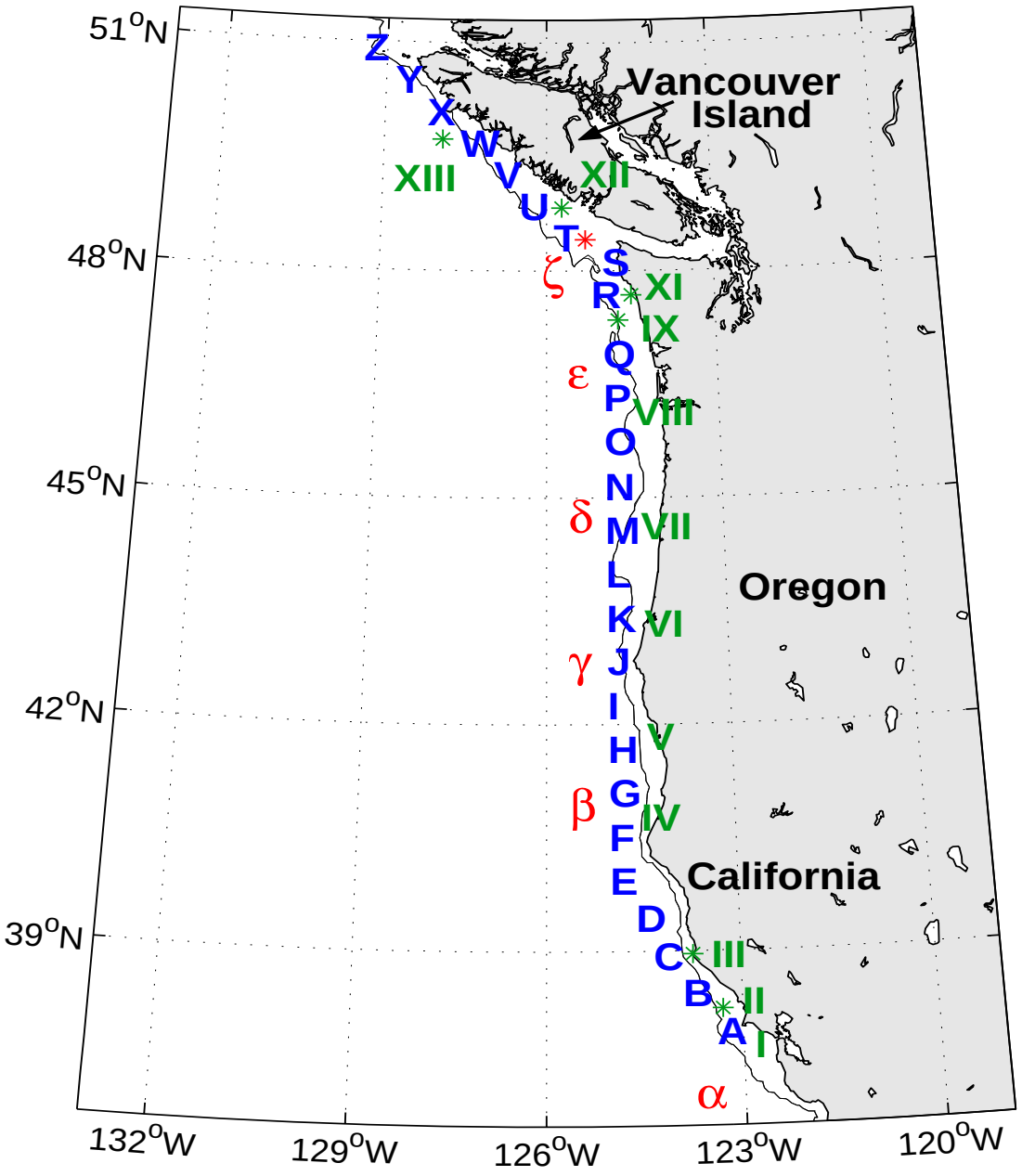

Figure 1: Data Locations

Locations extracted from (a) North American Regional Re-Analysis (NARR) (letters), (b) National Center for Environmental Predication (NCEP) Re-analysis (greek letters), and Observational data (roman numerals) used in this study. Exact locations are listed in Table 1. The 200 m isobath roughly indicates the shelf break.

system of grids using a three-dimensional forecasting model. These reanalysis data are produced by the National Center for Atmospheric Research (NCAR) and derived from Global Reanalysis data generated by NCEP. Global reanalysis data are developed using continuously refined land-surface models on a 180 km-wide grid [Mesinger, 2005]. The NARR project downscales NCEP outputs to regional-scale models with a finer 32 km grid. While wind data from NARR have failed to capture the declining trend in observed surface winds over the contiguous United States [Pryor et al., 2009], they compare more favourably with observations over coastal areas, agreeing to within 2 m/s and 31° direction [Moore et al., 2008].

NARR data were chosen from 26 locations roughly lining up with the shelf break along the entire study area, and were extracted at a 3-hourly time step from the beginning of the record (1979) to 2010. Spacing between each NARR location was 0.5° (~32 km) to ensure that wind data were derived from a unique grid cell. NCEP grid cells were chosen based on their proximity to the continental shelf. The coarser NCEP (2.5 x 2.5º) grid may obscure coastal wind phenomena [Bakun et al., 2010], but the data were included due to their superior temporal coverage, from 1948 to 2010.

Comparisons between model data derived from NCEP and observations off the coast of Vancouver Island and Washington state found that wind speeds differed by 1.6 – 4.5 m/s, wind direction was biased clockwise by 35° in the fall, and wind orientation was biased clockwise by 13° and 9° during the summer and fall, respectively [Tinis et al., 2006]. A substantial mismatch in the orientation or

Table 1: Names and coordinates of data sources.

Station	Latitude (° N)	Longitude (° W)	WMO Buoy
	Observational Stations		
XII	49.73	-127.92	c46132
XI	48.83	-125.99	c46206
X	47.68	-124.49	desw1
IX	47.35	-124.73	u46041
VIII	46.14	-124.51	u46029
VII	44.64	-124.5	u46050
VI	43.34	-124.38	caro3
V	41.85	-124.38	u46027
IV	40.78	-124.59	u46022
III	38.96	-123.74	ptac
II	38.24	-123.3	u46013
I	37.76	-122.83	u46026
	North American Regional Reanalysis data		
Z	50.91	-129.45	
Y	50.5	-128.83	
X	50.09	-128.21	
W	49.68	-127.59	
V	49.27	-126.96	
U	48.86	-126.34	
T	48.45	-125.72	
S	48.08	-125	
R	47.5	-125	
Q	46.91	-125	
P	46.33	-125	
O	45.75	-125	
N	45.16	-125	
M	44.58	-125	
L	44	-125	

Station	Latitude (° N)	Longitude (° W)	WMO Buoy
K	43.42	-125	
J	42.84	-125	
I	42.26	-125	
H	41.68	-125	
G	41.1	-125	
F	40.52	-125	
E	39.94	-125	
D	39.44	-124.6	
C	38.94	-124.2	
B	38.44	-123.8	
A	37.94	-123.4	
National Centers for Environmental Prediction data			
ζ	48.57	-125.63	
ε	46.67	-125.63	
δ	44.76	-125.63	
γ	42.86	-125.63	
β	40.95	-125.63	
α	37.14	-123.75	

direction of winds could result in a biased estimate upwelling and downwelling magnitude or occurrences.

A number of climate indices representing oscillatory climate behaviour are associated with the study area, including the El-Niño Southern Oscillation (ENSO), Pacific Decadal Oscillation (PDO), North Pacific Gyre Oscillation (NPGO), Northern Oscillation Index (NOI), Pacific-North America Oscillation (PNA), and the Arctic Oscillation (AO). ENSO, PDO, and NPGO have all been shown to influence alongshore winds and therefore nutrient availability throughout our study area [e.g., Ware and Thomson, 1991; Mantua et al., 1997;

Di Lorenzo et al., 2008]. Thus, these indices were used to consider the effect of climate variability on changes in onset, duration and intensity of upwelling and downweling seasons.

Monthly NPGO values from 1950-2010 were collected from http://www.o3d.org/npgo/. NPGO is a decadal-scale oscillation defined as the second Empirical Orthogonal Function (EOF) of Sea Surface Height anomalies (SSHa) over the eastern North Pacific Ocean (180°W - 110°W; 62°N - 25°N); a positive phase NPGO is associated with enhanced equatorward wind stress in the CCS at mid-low latitudes south of 38°N [Di Lorenzo et al., 2008].

Monthly PDO values between 1950 and 2010 were acquired from the Joint Institute for the Study of the Atmosphere and the Ocean Climate Data Archive (JISAO CDA) (http://jisao.washington.edu/data_sets/). The PDO is a decadal scale oscillation and is defined as the first EOF of Sea Surface Temperature anomalies (SSTa) in the Pacific Ocean north of 25°N; a positive PDO value indicates a deepening of the Aleutian Low pressure system off the southern coast of Alaska and enhanced poleward winds along the eastern Pacific Ocean coast [Mantua et al., 1997].

Monthly ENSO values from 1950 to 2010 were also collected from the JISAO CDA. ENSO is defined as the SSTa between the tropical (equatorward from 20°N and 20°S) and exotropical (poleward from 20°N and 20°S) Pacific Ocean [Penland et al., 2010]. An El Niño (positive) phase of ENSO is generally characterized by abnormally low pressure south of Alaska beginning in Northern

Hemisphere winter, leading to enhanced poleward winds throughout our study area [Rasmusson and Wallace, 1983; Hsieh et al., 1995].

2.2 Calculating Alongshore Stress

The magnitude of alongshore wind stress (AWS) is related to coastal winds by [Pond and Pickard, 1981]:

$$\tau = \rho_a C_d V^2 , \tag{1}$$

where $\tau \ \mathrm{N\,m^{-2}}$ is the wind stress exerted by the component of the daily average wind speed, $V \ \mathrm{m\,s^{-1}}$, parallel to the coastline; $\rho_a \ \mathrm{kg\,m^{-3}}$ represents air density; and C_d is a dimensionless drag coefficient argued by Trenberth et al. (1990) as

$$C_d = \begin{cases} 0.49 + 0.065V & \text{for } V > 10\ \mathrm{ms^{-1}} \\ 1.14 & \text{for } 3\ \mathrm{ms^{-1}} \le V \le 10\ \mathrm{ms^{-1}} \\ 0.62 + 1.5V^{-1} & \text{for } \mathrm{V} \le 3\ \mathrm{ms^{-1}} \end{cases} . \tag{2}$$

Upwelling is driven by the alongshore component of the wind speed. The Principal Axis of Rotation (PAR) was calculated at each location and defined as the local coastline orientation (Table 2), following similar analyses [e.g., Tinis et al., 2006; Garcia-Reyes and Largier, 2010].

2.3 Demarcating Seasons

Estimating wind stress using Equation (1) for all stations on a daily time step shows a clear seasonal signal, where downwelling favourable winds

pervade during winter months and upwelling favourable winds dominate during the summer (Figure 2a). The summer season was therefore defined here as the time-period of persistent upwelling-favourable winds (as shown by the calculated alongshore wind stress), while the winter is defined as the time period between successive summer seasons where downwelling-favourable winds persist.

The onset and conclusion of the upwelling season were assessed using the total cumulative AWS over an annual period (e.g. Figure 2b). To reduce the contribution of high-frequency variability, we applied a 30-d running average (RA) to the daily-wind stress data before estimating the total cumulative AWS. We then estimated the season onset and conclusion by associating them with a percentage of the total cumulative AWS for the year. For example, summer onset was associated with 10% of the total cumulative annual negative AWS from 1 January, with the conclusion associated with 90%. We refer to these values as the cut-off percentages (COP). The same estimates were made for the onset and conclusion of downwelling seasons using instead the total cumulative positive AWS occurring between two summers. For example, the winter onset is associated with 10% of the total cumulative positive AWS occurring between the last day of the preceding summer and the first day of the following proceeding summer.. A snapshot of 5 years of 30-d running mean alongshore wind stress at location U illustrates the performance of the criteria in selecting the onset and conclusion of both upwelling and downwelling seasons (Figure 2a). Figure 2c and 2d show examples of the estimation for summer onset and duration for location U for the entire data set. The spring transition is simply defined as

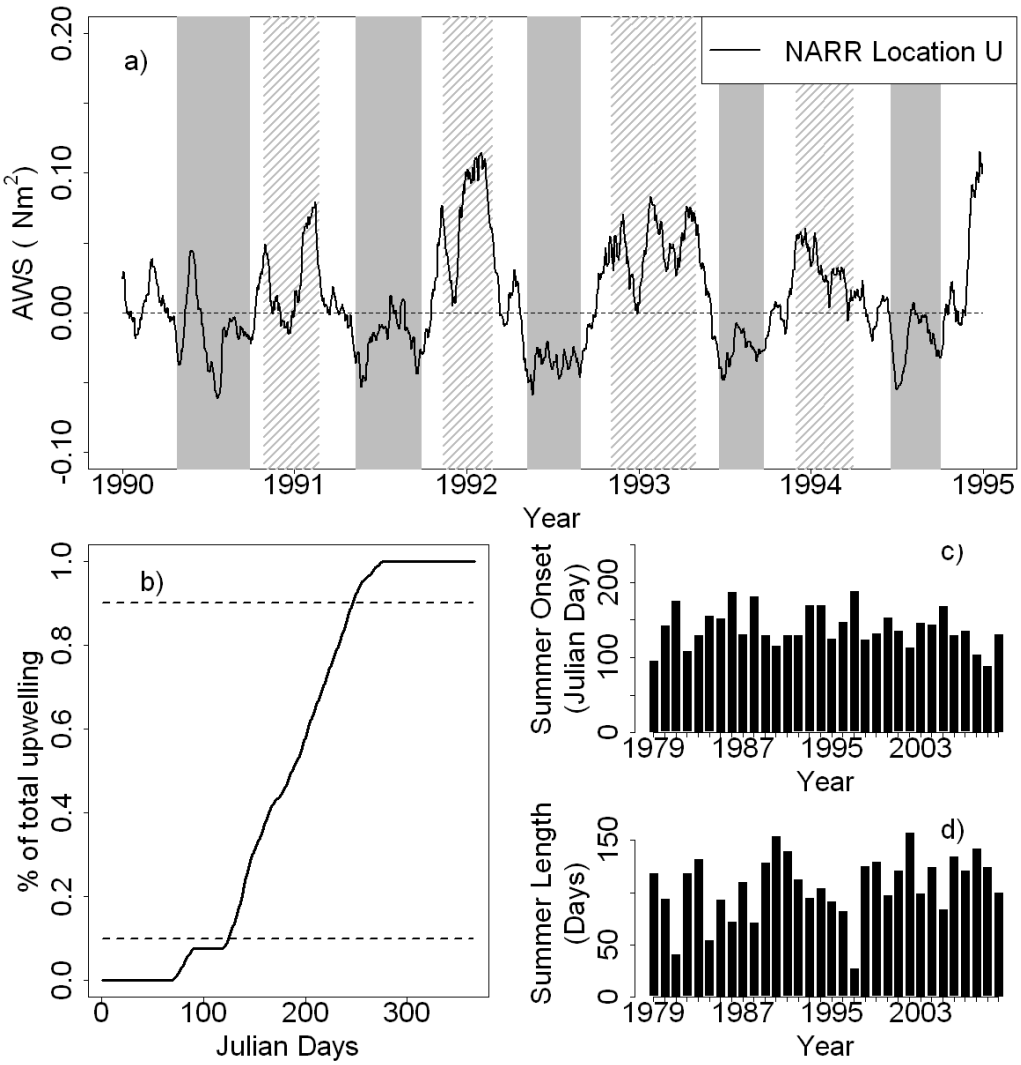

Figure 2: Example AWS, and onset criteria at location U

a) 5-year snapshot of 30-d running average (black line – negative indicates upwelling favourable wind, positive indicates downwelling-favourable) alongshore wind stress (AWS) at a typical NARR location, U, off Vancouver Island) to illustrate the performance of the objective demarcation criteria. Grey shading shows the summer (upwelling) season, while hatched shading indicates winter (downwelling) season. Seasons were determined using the criteria outlined in Section 2. b) the percentage of cumulative total upwelling during 1992 at station U as a function of time (days). Dashed line indicates the 10% and 90% cut-off percentages used to identify upwelling onset and conclusion, respectively. c) outcomes for summer onset (Julian Day) and d) summer duration (in days) using demarcation criteria outlined in Section 2 for station U.

starting at the end of the winter downwelling season and ending at the beginning of the summer upwelling. Similarly fall transition begins when summer upwelling ends and concludes at the onset of winter downwelling.

Sensitivity of seasonal onset to the choice of RA and COP were analyzed at NARR locations A, K, and W. The onset of summer start at location A using RAs ranging from 5 to 60 d showed little sensitivity (Figure 1 of Appendix A); however locations W and K did experience a later average start time with increasing RA, up to 30 d (Figures 2 and 3 in Appendix A). The onset of summer was sensitive to different choices of COP at all three locations (Figures 4, 5 and 6 in Appendix A). For example, the summer onset at station A was predicted to occur on average in late January for a COP of 2% and the middle of April for a COP of 16% (Figure 4 in Appendix A). An RA of 30 d and COP of 10% were chosen as a compromise which would minimize the influence of individual storm systems on the determination of seasonal onset without losing the ability to resolve seasonality completely. Sensitivity analyses also confirmed that varying the time at which to start adding up annual negative AWS by even three months had little effect on the ultimate choice of summer onset.

2.4 Time Series Analysis

In order to summarize the results from all 26 NARR locations succinctly, the time series of onset, duration and intensity (both upwelling and downwelling) of all four seasons (summer upwelling, fall transition, winter downwelling and spring transition) for each NARR station were grouped together using a hierarchical cluster analysis (the hcluster function in the R programming

language)[R Core Team, 2012]. Intensity for the purposes of this study is defined as the total upwelling or downwelling favourable wind stress integrated over the season in question. The hcluster algorithm clusters the data from different stations based on a Euclidean distance within the parameter space [Lucas and Jasson, 2006]. The physical meaning of the groupings calculated by hcluster must therefore be determined by the observer.

The end result is a dendrogram of progressively more similar data sets. The finals groupings presented here were chosen as the four main branches of the dendrogram produced by hcluster. Timing, duration, and intensity results were each grouped separately. The time series within each group determined by hcluster were averaged together, producing one time series per cluster.

Time series of the ENSO, PDO, and NPGO indices were compared to the clustered NARR time series of season onset, duration, and intensity via correlation analysis. Similarly, we compared these indices to the season onset, duration and intensity estimated from the NCEP derived wind data using the same criterion described above. Each of the climate indices (NPGO, PDO, and ENSO) were converted from monthly to annual values by averaging the indices over a calendar year. The yearly index values were then correlated to annual values of season onset, duration, and intensity for each season and examined for significance using Pearson's R test.

3: RESULTS

3.1 Assessing NARR and NCEP Data Relative to Observations

The PAR values derived from observational, NARR, and NCEP data sources are in close agreement with each other for a given latitude (Figure 3a; Table 2) and follow the orientation of the coast as expected (e.g. NW-SE orientations off northern California and Vancouver Island). The PAR values from the coarser NCEP data have a particularly smooth transition between locations compared to those generated from the NARR and observational wind data. The NARR and observation locations are closer to shore, and the more abrupt transitions could be due partially to topographic effects on wind. The PAR values estimated using NARR data differ from the nearest available observations by an

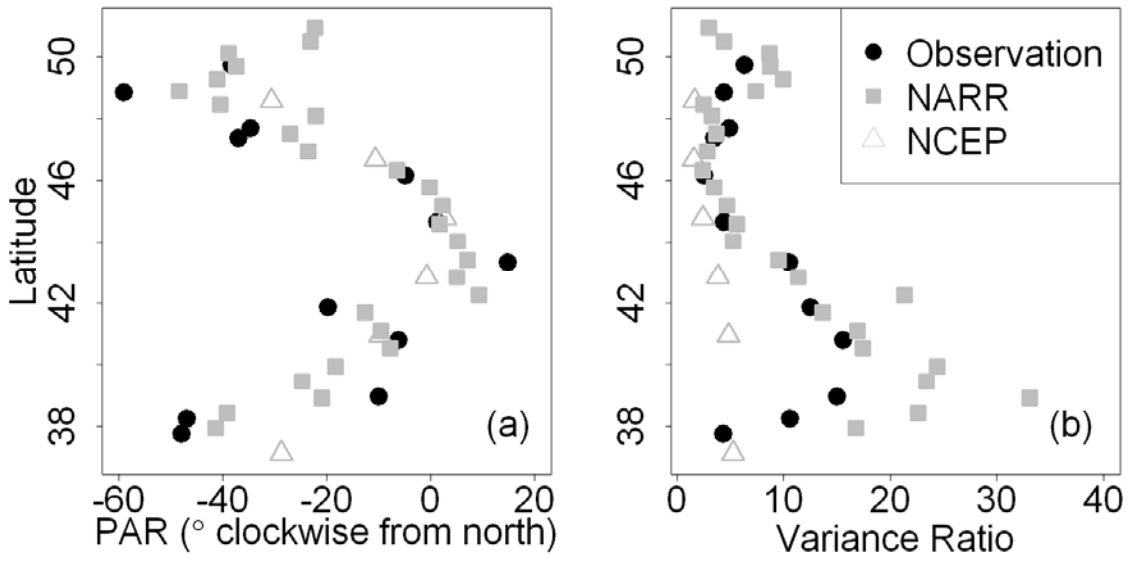

Figure 3: Principal Axis Rotations and Variance Ratios
Comparison between observation (circles), NARR (squares) and NCEP (triangles) derived estimates of (a) PAR and (b) Variance Ratio.

average of 7°, with a range from 0° - 12°. The PAR values from NCEP data differ from observations by 15° on average, ranging from 1° - 29°. The VR values for NCEP data are generally much lower than the VR values calculated for either NARR or observational datasets (Figure 3b; Table 2). The differences between NARR and nearby observational VR values are negligible between 40° N and 48° N, except at NARR location I (42.26°N), which has a much higher VR than observational location V (41.95°N). Winds are most isotropic for all locations near 46° N, off the north Oregon coast. The VR values from the NARR data show more anisotropy, i.e. a stronger principal axis, than observations at the northern and southern ends of the study area, especially south of 39° N where VR values from NARR achieve a 3-fold increase in VR compared to observations (Figure 3b). The coastline topography could be affecting the southernmost 3 observation locations, which are nearer to the shore than NARR locations A-C.

Table 2: Principle Axis Rotation (PAR) and Variance Ratio (VR) comparison between observation and select NARR and NCEP locations

Observation			NARR			NCEP		
Location	**PAR**	**VR**	**Location**	**PAR**	**VR**	**Location**	**PAR**	**VR**
XII	142	6.36	W	142	8.91	-	-	-
XI	121	4.43	U	132	7.16	ζ	150	1.64
X	145	4.91	R	152	3.61	-	-	-
IX	143	3.52	Q	155	2.97	ε	166	1.61
VIII	175	2.57	P	178	3.56	-	-	-
VII	1	4.44	M	2	5.68	δ	0	2.58
VI	15	10.51	J	5	11.63	γ	179	4.16
V	160	12.56	H	167	14.92	-	-	-
IV	174	15.57	G	171	16.88	β	171	5.09
III	170	15.04	C	159	32.88	-	-	-
II	133	10.64	A	138	17.51	-	-	-
I	132	4.37	-	-	-	α	150	5.09

A comparison between observed absolute wind speed, wind direction, and AWS for NARR and NCEP values showed stronger correlations between NARR and observations than NARR and NCEP (Table 3). The NARR and NCEP wind directions are well correlated to nearby observations for all locations and always more correlated than are wind speeds at NCEP and observational locations. One noticeable and unexplained exception to the overall strong AWS correlation performance (R ~ 0.9) occurs between observational location VIII (46.14°N) and NARR location P (46.33°N) (for AWS R=0.46). Correlating observation location VIII with the next closest NARR station, O (45.75°N), gave similarly low results (for AWS R=0.45) (Table 3).

Table 3: Correlation of winds between observation and nearby NARR and NCEP locations

	NARR				NCEP			
Observation Locations	**Location**	**Wind Speed**	**Wind Dir**	**AWS**	**Location**	**Wind Speed**	**Wind Direction**	**AWS**
XII	W	0.83	0.90	0.90	-	-	-	-
XI	U	0.83	0.83	0.88	ζ	0.72	0.82	0.82
X	R	0.82	0.80	0.89	-	-	-	-
IX	Q	0.86	0.90	0.92	ε	0.70	0.83	0.83
VIII	P	0.78	0.90	0.46	-	-	-	-
VII	M	0.90	0.92	0.94	δ	0.76	0.86	0.86
VI	J	0.77	0.86	0.85	γ	0.61	0.69	0.69
V	H	0.81	0.81	0.88	-	-	-	-
IV	G	0.86	0.88	0.92	β	0.73	0.83	0.83
III	C	0.77	0.75	0.89	-	-	-	-
II	A	0.90	0.83	0.91	-	-	-	-
I	-	-	-	-	α	0.74	0.84	0.84

3.2 Demarcating Seasons

Demarcating upwelling and downwelling seasons based on criteria outlined in Section 2 captures the bimodal behaviour of coastal winds over an

annual cycle in our study area (e.g., Figure 2). The performance of the demarcation criteria was evaluated with a Student's t-test between the choice of season start and duration from station U (48.86°N) using our method, and the results of Thomson and Ware (1996) (hereafter referred to as TW96) at nearby La Perouse Bank (station XI at 48.83°N), between 1987 and 1995 (Table 4). A direct comparison with TW96 upwelling index must include a small caveat, since the upwelling index is based on actual current measurements. Some upwelling events in this part of the study area are generated via coastal trapped waves originating as far south as southern California, and cannot be captured by examining local wind behaviour alone [Winant and Olson, 1976]. We therefore expect some discrepancies (e.g., a shorter summer upwelling season using our criteria) between our criteria and the index developed in TW96.

Table 4: Results for season onset and duration compared to Thomson and Ware, 1996 (TW96).

		Summer Onset			Summer Length		
	Season	Mean (Julian Day)	SD	t-test	Mean (Days)	SD	t-test
TW96	SP	51	15	-	76	36	-
	SU	140	30	-	144	32	-
	FA	289	30	-	65	27	-
	WI	356	28	-	52	29	-
Location U	SP	77	22	0.07	62	14	0.44
	SU	138	20	0.92	118	22	**0.04***
	FA	256	20	0.06	59	24	0.50
	WI	315	17	0.06	127	27	**0.00***
Location M	SP	72	23	0.15	63	16	0.48
	SU	135	21	0.69	131	18	0.44
	FA	266	18	0.26	54	15	0.34
	WI	320	11	0.07	118	26	**0.00***

While the average start dates of summer upwelling are almost identical for the two stations, the average summer durations estimated using our demarcation method are significantly shorter (significant at the p = 0.05 level). On average, the whole fall season is shifted earlier, with the end of summer upwelling occurring 36 days earlier and the beginning of winter downwelling starting 42 days earlier. Our demarcation criteria also result in a later end to the winter downwelling season, and leads to a significantly (74 days) longer winter season, on average.

Results for season onset and duration from TW96 were also compared to location M off the coast of Oregon. Interestingly, the results at location M more closely matched those from TW96 than location U, as indicated by the larger p-values for six out of eight metrics. The duration of winter was still significantly longer (although shorter than station U), and the summer onset was slightly earlier than at location U. A key difference between results for location U and M is the later fall onset at location M, which effectively stretches out the duration of its summer. In fact, the fact that the summer duration at location M is in much closer agreement with TW96, which may be the result of the coastal trapped waves propagating from the Oregon coast to the TW96 location [Hickey, 1979].

3.3 Cluster Analysis of NARR Data

Hierarchical clustering was initially performed on data from all NARR locations for season timing, duration, and upwelling and downwelling intensity. The clustering results for season timing and duration at the second branching stage were identical, except for location J, which switched from group 2 to group

3 for the duration of all four seasons, respectively. The clustering results of season start were therefore also used to group the season duration time series (Figure 4a). The grouping of NARR stations by upwelling and downwelling intensity on the other hand was significantly different (Figures 4b and c).

Clusters were generally grouped by latitude (dendrogram plots for clusters available in Figures 19 through 22 of Appendix A). Locations north of 50°N (Y-Z) were consistently grouped together, and experienced longer, more intense downwelling seasons, and shorter, lower intensity upwelling seasons (Figure 5).

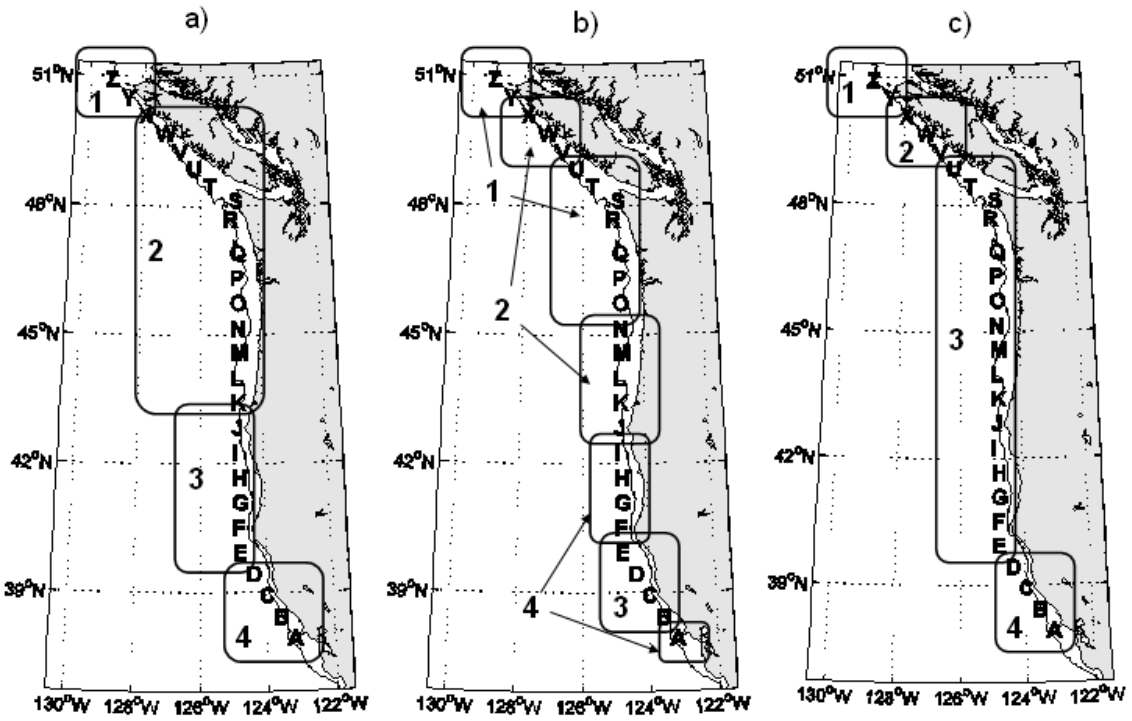

Figure 4: Hierarchical clustering results

Hierarchical clustering results for all four seasons for a) season onset and duration, b) upwelling intensity, and c) downwelling intensity. Season onset and season duration produced almost identical results in the clustering analysis (Station J was included in cluster 2 for all four season durations).

.The main branches of the clusters were divided at roughly 43°N, except for downwelling intensity (Figure 22 of Appendix A). While downwelling intensity

generally increases in the more northern locations (Figure 5b), the relatively large cluster extending from 40-50°N in downwelling suggests that downwelling exhibits more consistent behaviour than upwelling through the region. This inference is supported by clustering results which show that locations 40-42°N (E-G) and 47°N+ (Q and T) are more similar to each other than locations H-P (Figure 22 of Appendix A) Downwelling becomes infrequent enough by cluster 4 as to not even register any downwelling events, leading to gaps in the time series (Figure 5b,d,f). Except for upwelling intensity, locations south of 40°N (A-D) were always clustered (Figure 4a and 4c). The length of summer of summer (winter) generally decreases (increases) with increasing latitude (Figure 5e,f).

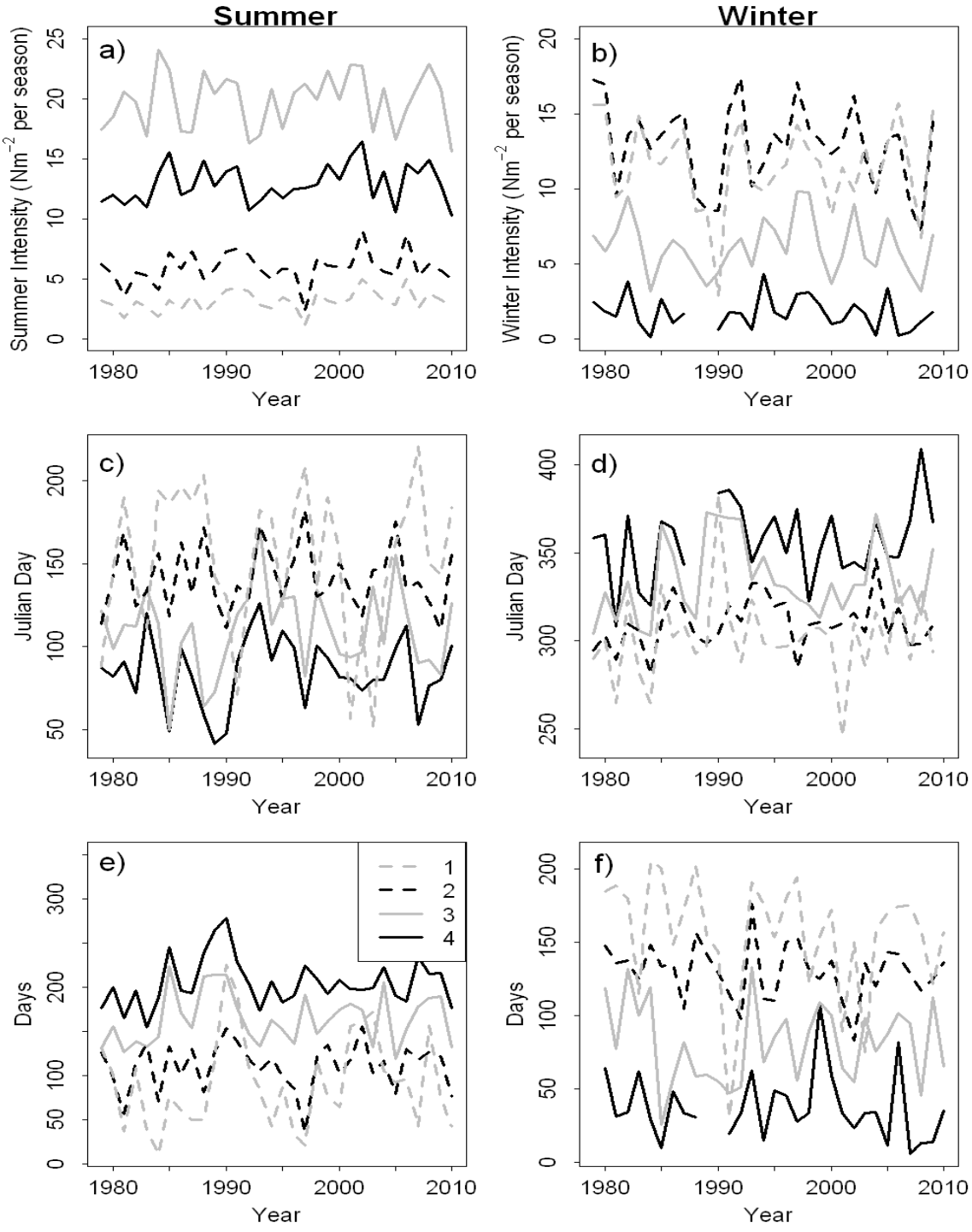

Figure 5: Cluster time series results

Time series of onset and duration clusters 1 (black solid line), 2 (grey solid line), 3 (dashed black line), and 4 (grey dashed line) for summer a) upwelling intensity, c) onset, and e) duration, and winter b) downwelling intensity, d) onset, and f) duration.

3.4 Temporal trends in onset, duration and intensity of alongshore winds

There were no statistically significant linear temporal trends for the onset, duration or intensity for any season other than summer for NARR data (regressions not shown; time series found in Figures 7 through 18 of Appendix A). Five NARR locations showed a significant trend towards higher upwelling intensity with time (Figure 6), including two sites off northern California (F and G, at the $p = 0.01$ level) and three sites off northern Washington and southern Vancouver Island (R and U at the $p = 0.01$ level; T at the $p = 0.05$ level). Comparing the time series of upwelling intensity between locations D, E, F, G, and H off northern California shows that the significant trend in F and G is mostly due to enhanced wind-driven upwelling observed between 2003 and 2010 (Figure 6a).

Trends in NCEP time series data tell a different story. Simple linear regression of data from locations α, near central California, and δ, ε and ζ, extending from central Oregon to northern Washington, all indicate a trend towards a significantly later start of summer at the $p = 0.05$ level (Figure 7a). These linear trends are misleading, however, as there is a step toward longer summer seasons in each time series during the 1977-1978 PDO regime shift (red vertical line in Figure 7). The step at 1977-1978 is statistically significant at the $p=0.05$ level using the Rodionov regime shift algorithm [Rodionov, 2004]. The

1948-1977 and 1978-2010 means of summer onset are also significantly different

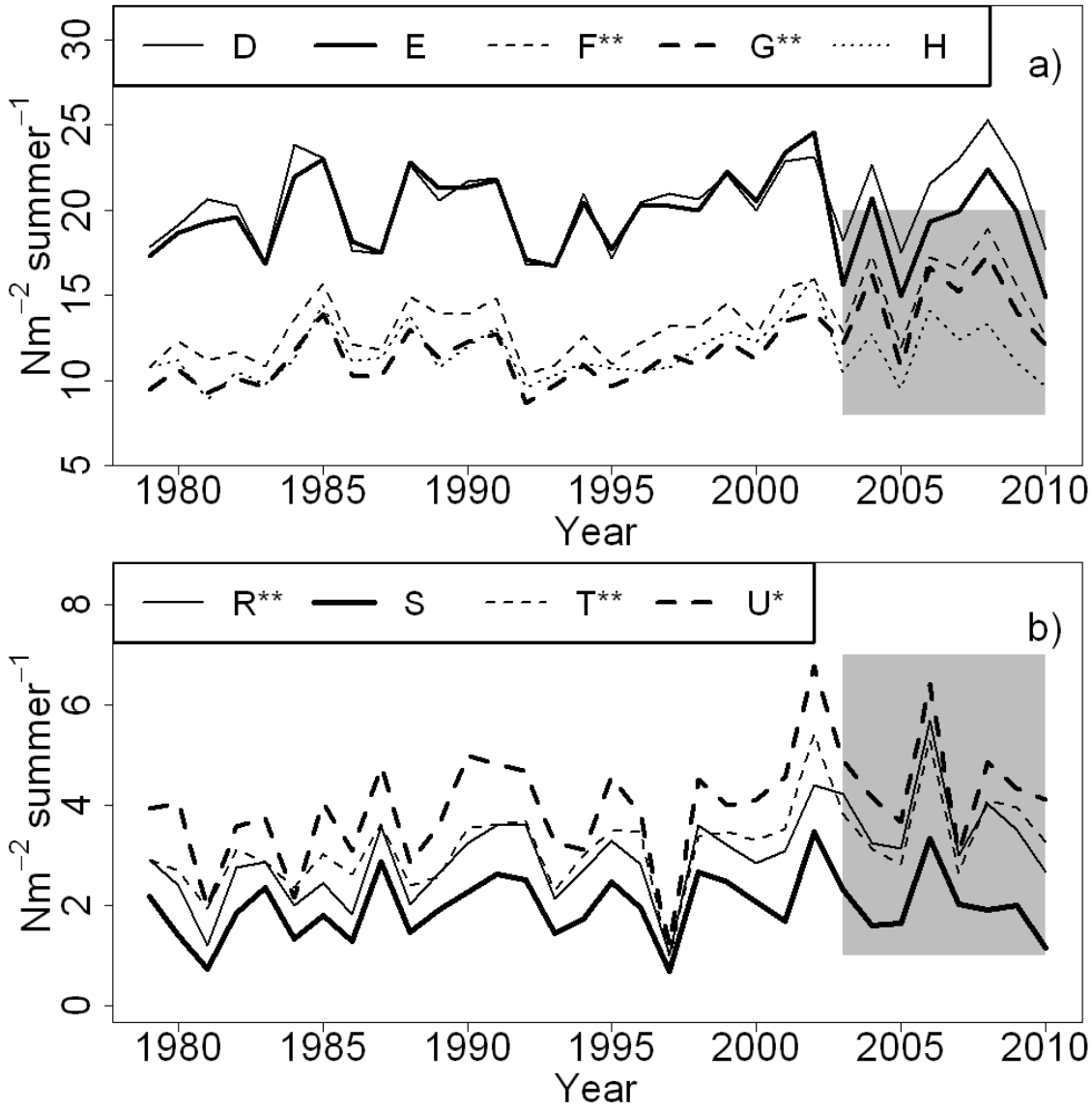

Figure 6: NARR Time Series Analysis

a) time series of summer upwelling intensity for locations D through H; b) time series of upwelling intensity for locations R through U. Stars denote time series with a significant trend of more intense upwelling with time at the p = 0.01 level (**) and p= 0.05 level (*). Note the different scale for the vertical axis for (b).

at the p = 0.05 level for NCEP locations α, δ, ε and ζ (Table 5).

NCEP data also reveal a more complex picture of summer upwelling intensity than that detected in the NARR time series analysis (Figure 7b)

indicating the importance of having a time series longer than a few decades. Location β in northern California appears to have increasing upwelling intensity between 1948 and 1965, and again from roughly 1997 to 2010. Between these two intervals, location β shows a slight decreasing wind-driven upwelling intensity trend. The mean upwelling intensity at location β before 1979 is only 0.12 Nm-2, less than upwelling intensity after 1979. It should be emphasized again that there was no significant trend in time series for upwelling intensity for any season for all six NCEP locations.

Table 5: T-test of means before and after 1977-1978 PDO regime shift

	Mean (Julian Day)		
Station	**1948-1977**	**1978-2010**	**t-test p-value**
α	69	83	**0.011**
β	105	116	0.052
γ	124	137	**0.033**
δ	136	150	**0.011**
ε	131	152	**0.001**
ζ	122	149	**0.002**

Bold station names on the left denote significant differences in the means at the p = 0.05 level.

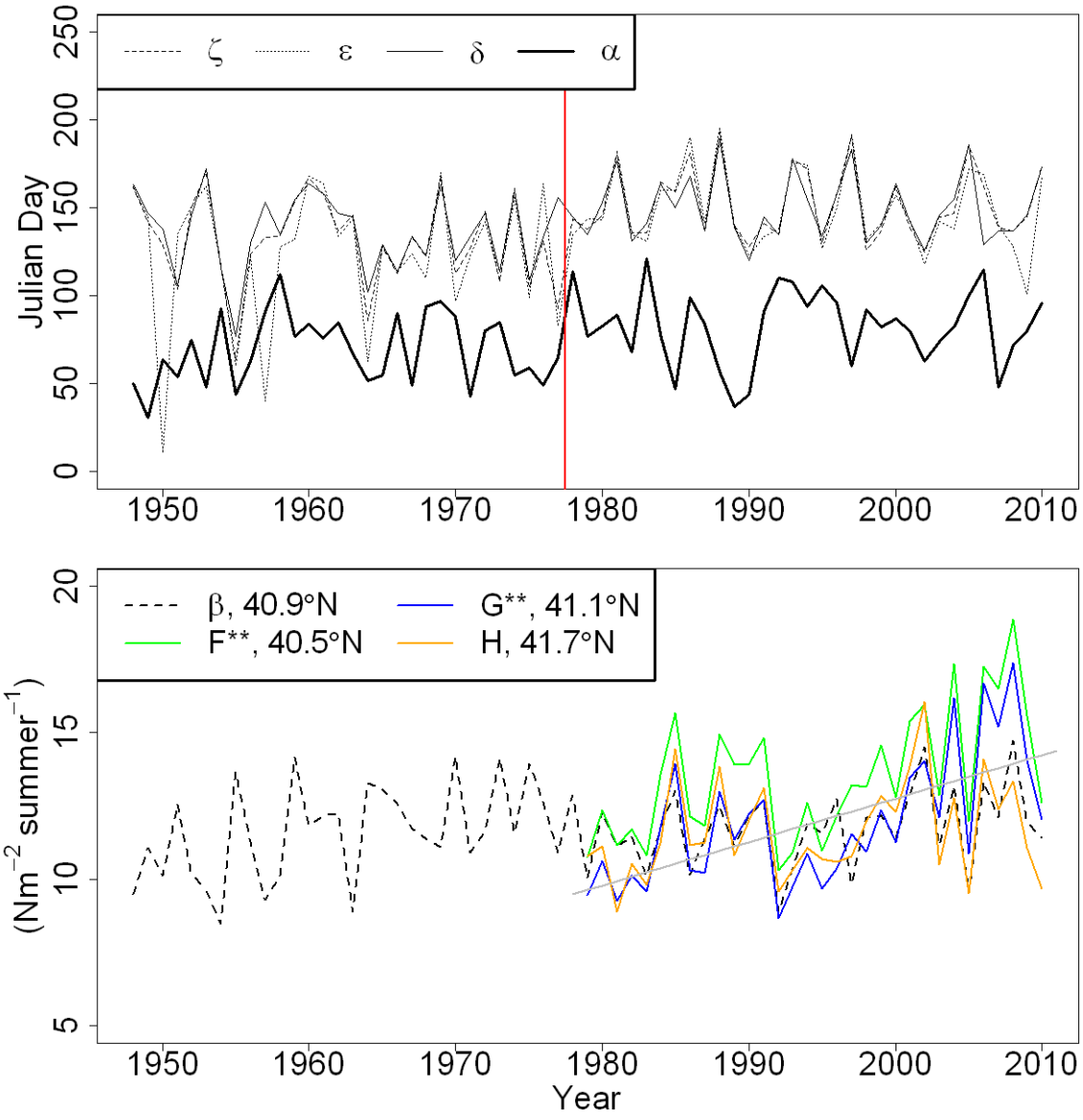

Figure 7: Comparison between NARR and NCEP summer intensity time series

a) time series of summer onset at NCEP locations α (dark solid line), δ (thin solid line), ε (dotted line), and ζ (dashed line), all of which show statistical trends at the p = 0.01 level; b) comparison between time series of upwelling intensity between NCEP location β dashed line and nearby NARR locations F (green line), G (blue line), and H (orange line). Stars in legend denote significance at the p = 0.01 level. The grey line is the simple linear regression with time at NARR location G.

3.5 Correlations to climate oscillations

3.5.1 Correlation between NARR clusters and climate indices

The NARR time series for onset, duration, and intensity were most often uncorrelated to NPGO, ENSO, or PDO (Table 6). However, some correlations do present themselves for each index and are discussed below.

NPGO is most related to oceanographic changes south of 38°N [Di Lorenzo et al., 2008], and significant correlations further north were not expected. We found that NPGO has a weak negative correlation to summer onset for NARR locations south of 43°N, meaning an earlier onset of summer upwelling is associated with the positive phase of NPGO (Table 6a). The onset of the spring transition is also negatively correlated to NPGO between 40 and 43°N (Table 6a). The earlier onsets do not correspond to any significant correlations between NPGO and duration for any season (Table 6a). Summer upwelling intensity at NARR locations is negatively correlated to NPGO between 38 and 42°N (Table 6c). Therefore, during the positive (negative) phase of NPGO, upwelling intensity is enhanced (reduced) off the coast of Northern California and Southern Oregon.

The PDO is positively correlated with summer onset at cluster 2 (43 – 50.5°N) (Table 6a), and indicates that the positive phase of the PDO is associated with a delayed onset of summer upwelling. The PDO is also negatively correlated with summer duration throughout the whole study area (Table 6b), meaning that the summer upwelling season along the northern CCS is relatively shorter during a positive phase of the PDO. Summer upwelling intensity is positively correlated to the PDO between 38 and 42°N (Table 6c).

Table 6: Correlation between NPGO, PDO, and ENSO indices, and NARR clusters

	NPGO				PDO				ENSO			
Cluster	**SU**	**FA**	**WI**	**SP**	**SU**	**FA**	**WI**	**SP**	**SU**	**FA**	**WI**	**SP**
					a) Season Onset							
1	-0.11	0.03	-0.19	-0.28	0.17	**-0.39**	-0.20	0.19	-0.20	-0.21	0.06	-0.16
2	-0.20	0.00	-0.28	-0.35	**0.39**	-0.13	0.04	**0.38**	0.00	0.09	0.18	-0.03
3	**-0.42**	-0.10	-0.28	**-0.40**	0.31	-0.17	-0.15	0.25	**0.39**	0.06	0.07	**0.36**
4	**-0.35**	-0.18	-0.03	-0.09	0.31	-0.23	**-0.45**	0.08	0.34	0.01	-0.11	0.15
					b) Season Duration							
1	0.12	-0.29	-0.17	0.12	**-0.40**	**0.42**	0.21	0.06	0.02	**0.42**	-0.20	-0.14
2	0.15	-0.35	-0.25	0.23	**-0.36**	0.23	0.23	-0.04	0.06	0.13	-0.15	0.07
3	0.31	-0.29	-0.12	0.11	**-0.36**	-0.02	0.13	0.00	-0.30	0.04	0.12	-0.07
4	0.16	0.13	-0.03	-0.22	**-0.37**	-0.31	0.07	0.08	-0.25	-0.18	-0.05	0.04
					c) Upwelling Intensity							
1	-0.10	0.13	-0.06	-0.23	0.24	0.01	-0.16	0.13	-0.03	-0.08	0.24	0.01
2	-0.04	0.07	0.08	-0.14	0.17	-0.12	-0.21	0.20	-0.04	-0.07	0.07	-0.04
3	**-0.33**	-0.08	0.09	-0.11	**0.35**	**0.32**	-0.08	0.06	**0.28**	0.09	-0.07	0.06
4	**-0.37**	0.01	0.05	-0.08	**0.34**	0.14	-0.15	0.09	**0.25**	0.04	-0.09	0.07
					d) Downwelling Intensity							
1	0.29	-0.07	-0.26	0.35	**-0.42**	0.17	**0.41**	0.05	-0.09	0.33	**0.44**	-0.20
2	0.15	-0.12	-0.28	**0.38**	-0.35	0.15	0.34	-0.07	0.10	**0.42**	**0.54**	-0.08
3	0.03	-0.25	-0.35	0.08	-0.25	0.06	0.26	0.17	-0.08	0.21	**0.59**	0.14
4	0.00	0.02	-0.25	-0.13	-0.09	-0.01	-0.05	0.05	-0.04	0.13	0.26	0.30

SU = summer, FA = fall, WI = winter, SP = spring
Bold denotes significance at the p = 0.05 level.

Similarly, a positive PDO phase is positively correlated with winter downwelling intensity, but at northern Vancouver Island.

ENSO is positively correlated to summer and spring onset between 40 and 43°N (Table 6a), suggesting that the onset of spring and summer seasons occur later in the positive El Niño phase of ENSO. In contrast, upwelling intensity is negatively correlated to ENSO between 38 and 42°N (Table 6c), meaning that this region experiences lower upwelling intensities during El Niño years. Most prominent is the positive correlation between ENSO and downwelling intensity between 40 and 52°N (Table 6d), suggesting that the positive (El Niño) phase brings enhanced downwelling in the northern part of the study area..

In summary, our analysis of correlations between climate indices and onset, duration, and intensity of wind-driven upwelling and downwelling at NARR locations indicate that: 1) correlations are few between wind behaviour and NPGO, ENSO, and PDO according to NARR data in our study area; 2) the positive phase of the NPGO is associated with less intense summers which begin later than normal between 38 and 42°N; 3) the positive phase of the PDO is correlated with shorter summer upwelling seasons across the study area, but only less intense upwelling between 38 and 42°N; and 4) the El Niño phase of ENSO is associated with less summer upwelling between 38 and 42°N and more winter downwelling between 40 - 52°N.

3.5.2 Correlation between NCEP locations and climate indices

Correlations between NCEP season onset, duration and intensity and the climate indices are somewhat more revealing. The spring and fall transition seasons are still often uncorrelated to NPGO, ENSO, and PDO. It is the summer and winter seasons which show some connection to basin-scale climate oscillations.

Correlations between the NCEP data and the NPGO index are negative for the summer and spring onset south of 42°N, indicating that both start earlier during positive phases of the NPGO (Table 7a). Fall duration between 43 and 52°N is also significantly negatively correlated to the NPGO, and indicate a shorter fall transition during positive NPGO phases (Table 7b). Significant negative correlation between NPGO and upwelling intensity indicates enhanced upwelling during positive NPGO phases, and occurs during the summer south of 43°N and off the Vancouver Island, Washington, and Northern California coasts during the spring (Table 7c). Downwelling intensity is negatively correlated with NPGO off the Washington and Oregon coasts during the fall and winter. The only positive correlation between the NPGO index and the NCEP results occurs with downwelling intensity off the Vancouver Island and Washington coasts in the spring (Table 7d).

The PDO is negatively correlated to summer onset and positively correlated with duration throughout the study area (Tables 7a and b), suggesting that the positive (warm) phase of the PDO is associated with later and shorter summer upwelling seasons. PDO is also positively correlated with fall and winter

Table 7: Correlation between NPGO, PDO, and ENSO indices, and NCEP locations

	NPGO				PDO				ENSO			
Location	**SU**	**FA**	**WI**	**SP**	**SU**	**FA**	**WI**	**SP**	**SU**	**FA**	**WI**	**SP**
					a) Season Onset							
ζ	0.04	0.05	-0.15	-0.03	**0.50**	-0.15	0.04	**0.40**	**0.30**	-0.10	0.06	0.19
ε	-0.06	0.11	-0.23	-0.20	**0.48**	0.05	0.16	**0.35**	**0.29**	0.12	0.24	0.16
δ	-0.01	0.16	-0.11	-0.11	**0.49**	0.09	0.16	**0.35**	**0.31**	0.17	0.15	0.13
γ	-0.01	0.06	-0.16	-0.18	**0.36**	0.13	0.13	0.19	**0.26**	0.17	0.09	0.18
β	**-0.32**	-0.04	-0.15	**-0.41**	**0.26**	0.14	-0.03	**0.26**	**0.27**	0.15	0.07	**0.31**
α	**-0.28**	0.01	0.05	-0.02	**0.43**	-0.17	**-0.28**	0.25	**0.43**	-0.11	-0.14	**0.31**
					b) Season Duration							
ζ	-0.01	**-0.28**	0.00	0.14	**-0.53**	**0.29**	**0.37**	0.26	**-0.32**	0.25	0.09	0.22
ε	0.11	**-0.39**	-0.22	0.21	**-0.41**	0.13	**0.26**	0.21	-0.20	0.15	0.10	0.21
δ	0.10	**-0.30**	0.01	0.15	**-0.37**	0.08	0.19	0.16	-0.16	-0.01	-0.02	0.23
γ	0.05	**-0.28**	0.02	**0.30**	**-0.26**	0.04	-0.01	0.13	-0.14	-0.02	-0.04	0.04
β	**0.27**	-0.17	-0.10	0.26	-0.15	-0.15	0.00	-0.09	-0.15	-0.03	-0.05	-0.16
α	0.21	0.09	0.06	-0.15	**-0.42**	-0.23	**0.29**	0.06	**-0.38**	-0.14	0.18	-0.04
					c) Upwelling Intensity							
ζ	-0.01	0.15	-0.02	**-0.30**	**0.33**	-0.08	0.00	-0.01	0.16	-0.18	0.17	-0.06
ε	0.01	0.22	-0.06	**-0.26**	0.16	-0.05	0.16	-0.02	0.03	-0.15	**0.35**	-0.10
δ	0.00	0.18	-0.04	-0.09	0.17	-0.07	0.04	-0.05	0.03	-0.04	0.17	-0.17
γ	-0.08	0.14	0.08	-0.20	0.22	-0.11	0.23	-0.15	0.06	-0.05	0.20	-0.06
β	**-0.35**	0.05	0.05	**-0.28**	**0.30**	0.14	-0.13	-0.01	**0.30**	0.06	-0.07	0.08
α	**-0.43**	-0.24	0.04	0.00	**0.26**	**0.28**	**-0.38**	-0.02	**0.45**	**0.28**	**-0.29**	0.14
					d) Downwelling Intensity							
ζ	0.02	-0.24	-0.26	**0.40**	**-0.41**	**0.43**	**0.39**	0.15	**-0.32**	**0.54**	**0.56**	0.01
ε	0.18	**-0.35**	**-0.30**	**0.35**	-0.20	0.22	0.25	0.03	-0.16	**0.39**	**0.45**	-0.06
δ	0.07	**-0.26**	-0.25	0.24	-0.18	0.20	0.18	0.07	-0.13	0.24	**0.40**	-0.02
γ	-0.02	-0.16	**-0.28**	0.17	-0.07	0.14	0.23	**0.30**	0.01	0.16	**0.45**	0.12
β	0.13	-0.08	**-0.32**	0.03	0.13	-0.08	**0.31**	0.18	0.16	0.10	**0.49**	0.11
α	0.03	0.07	-0.18	-0.13	-0.09	-0.15	0.24	**0.27**	-0.05	-0.11	**0.41**	**0.27**

SU = summer, FA = fall, WI = winter, SP = spring
Bold denotes significance at the p = 0.05 level.

duration off the Washington coast (Table 7b). The PDO and upwelling intensity are positively correlated south of 42°N during the summer, fall and negatively correlated during the winter (Table 7c). Summer upwelling intensity is also positively correlated with location ζ (near Juan de Fuca Strait). PDO is negatively correlated with downwelling intensity at ζ during the summer, fall and winter (Table 7d).

Summer onset is positively correlated with ENSO throughout the study area (Table 7a), but summer duration is only significantly correlated to ENSO at α and ζ locations (Table 7b). Upwelling intensity is positively correlated to ENSO in central California during the summer and fall, and negatively correlated to ENSO in the winter. Downwelling intensity is prominently correlated to ENSO throughout the entire study area during the winter, but also off the Washington coast during the fall (Table 7d).

In summary, our analysis of correlations between climate indices and onset, duration, and intensity of seasons for NCEP locations indicates that 1) the positive phase of the NPGO is associated with earlier onset of summer upwelling with more intense upwelling off northern California and southern Oregon, shorter fall seasons between Oregon and Vancouver Island, and less downwelling during the winter between Vancouver Island and California; 2) the positive (warm) phase PDO is associated with later onset of summer and spring seasons and shorter summer upwelling seasons throughout the study area, less upwelling off the northern California coast during the summer and fall, and more intense downwelling near the Strait of Juan de Fuca during the fall and winter; and 3)

The positive (El Niño) phase of ENSO is associated with later summers throughout the study area, less upwelling off the northern California coast during the summer and spring, and more winter downwelling throughout the study area.

3.5.3 Comparison between NARR and NCEP Correlations with Climate Indices

The results of the correlations between climate and the NARR and NCEP data are generally in agreement. Two notable exceptions are the fall duration correlation with NPGO and the summer and spring onset correlation with PDO. While the NARR correlations for these variables were not significant compared to their NCEP counterparts, they are of the same sign as NCEP locations, and may therefore be an indication of a small sample size. The other notable exception is the summer onset correlation with ENSO. In this case, NARR locations north of 43°N suggest zero correlation, in contrast to NCEP locations which show significant correlations between ENSO and all stations up to the Juan de Fuca Strait.

4: DISCUSSION

4.1 Temporal Trends

Results from our analysis of NARR winds are mostly consistent with previous studies indicating no significant temporal trends in summer onset or upwelling duration north of 40°N from 1979 to 2010 [Schwing and Mendelssohn, 1997; Garcia-Reyes and Largier, 2010]. However, our results do suggest increasing trends in summer upwelling duration near southern Vancouver Island (NARR locations S, T, and U). These results should be treated with caution; most of the increase occurs after 2003 and is based on a simple linear regression which is unable to capture nonlinear interactions. The rate of increase in summer intensity for all three locations is -0.049 to -0.040 Nm-2 per year. If one assumes a drag coefficient of 0.0015 (Equation 1), then these increases are equivalent to an average increase in equatorward wind speed of ~0.05 m/s per year, during summer, or an impressive annual increase of roughly 2% per year in median wind speed. The same estimation yields ~0.06 m/s for near central California (locations F and G), which is similar to estimated changes in upwelling intensity previously found between 1982 and 2008 at 38°N [Garcia-Reyes and Largier, 2010]. Other estimates for changes in wind-driven upwelling intensity are as high as 0.15 m/s per year between 1946 and 1990 at 40°N, but are based on a static summer period of April-July [Schwing and Mendelssohn,

1997] as opposed to a more realistic, variable summer onset and duration used in our analysis.

The analysis of wind data from NCEP locations brings a new dimension to the discussion of upwelling-favourable winds along the CCS in two ways. First, the longer time series reveals the non-linear behaviour of summer upwelling intensity with time, and cautions the use of linear regression as a stand-alone diagnostic of temporal trends for time periods of a few decades or less.

Second, our analysis with the NCEP data illustrates the effect of changes in both temporal and spatial scales on resulting trends and correlations. The enhanced summer upwelling intensity trend at NARR locations F, G, R, T, and U are not present at the nearby NCEP locations β and ζ (Figure 7). On the one hand, the coarse resolution of NCEP data could be unable to capture the true magnitude of nearshore coastal winds, especially at the extremes. On the other hand, the NCEP time series are twice the length of NARR locations, and provide more information about the long-term behaviour of coastal winds in our study area. The PDO regime shift of 1977-1978 is apparent in NCEP time series north 42°N as a distinct step in the onset and duration of the summer season (Figure 7; Table 5). Such large-scale temporal oscillations as PDO are likely to bias conclusions based on shorter time series.

Both the NARR and NCEP data illustrate strong interannual variability in alongshore wind stress throughout the study area. We emphasize that this analysis considers only the wind-driven component of upwelling and downwelling, and has not considered the influence of stratification [Lentz and

Chapman, 2004] or coastal trapped waves [Hickey, 1979]. Such metrics are required to fully characterize the behaviour of the coastal waters, and ultimately determine the true magnitude of upwelling. Therefore, while locally wind-driven upwelling north of 40°N in the CCS may not be increasing during the summer, the enhanced upwelling measured further south in historical analyses and model predictions [e.g., Auad et al., 2006; Snyder et al., 2003] could still lead to enhanced upwelling through coastal trapped waves north of 40°N.

4.2 Implications of Correlations with Climate Indices

The positive phases of both the PDO and ENSO indices are associated with shorter, later summer upwelling seasons throughout the whole study region; however, their relationship with upwelling intensity is less pronounced north of 40°N (Table 7). The positive-phase of the PDO has been previously associated with a deepening of the Aleutian low pressure system, leading to decreased upwelling north of 38°N [Chhak and Di Lorenzo, 2007]. The behaviour associated with positive ENSO phases is similar, whereby anomalously low pressure is created south of Alaska through the warming of tropical surface water in the Pacific, generating more poleward winds through our study area [Rasmusson and Wallace, 1983]. While the positive phases of ENSO and PDO are linked to a delay and shortening of summer upwelling, they do not appear to significantly subdue the summer upwelling intensity (Tables 6c and 7c). In fact, given that the summer season becomes shorter during positive PDO and ENSO phases, late summer upwelling must be more intense than during a negative phase, to account for little change in upwelling intensity. A possible explanation

of this behaviour is that positive PDO and ENSO phases lead to a change in wind speed frequency, resulting in fewer but stronger pulses of upwelling. If PDO and ENSO patterns are expected to change through time (i.e., become positive more often), then one might anticipate delayed onsets of summer upwelling more often. A delay in summer upwelling is associated with a change in plankton assemblages, and a bottom-up effect on pelagic communities in general [Ware and Thomson, 2005; Barth et al., 2007; Bakun et al., 2010].

The negligible correlation between NPGO and alongshore winds north of 40°N is supported by previous work [Di Lorenzo et al., 2008]. However, NPGO appears to be related to enhanced winter downwelling in the study area (Table 7). This pattern is expected because a negative NPGO phase is indicative of an anomalously strong N-S pressure gradient resulting from a high pressure centered at ~ 30°N and150°W, with a deepening low centered at 55°N and 150°W. The resultant wind stress creates enhanced upwelling through equatorward winds along the Eastern Pacific Coast south of 38°N, and enhanced downwelling from poleward winds north of 40°N [Di Lorenzo et al., 2008].

The general lack of correlation between upwelling intensity and the NPGO, PDO, and ENSO indices north of 40°N is surprising, given the correlation in summer onset and timing to PDO, and to a lesser extent, ENSO (Tables 5c and 6c). Part of the reason could be in our working definition of upwelling intensity (see Section 2.3). A different metric which can explicitly quantify the magnitude or number of wind stress pulses might better elucidate this dynamic. Variance in the NPGO has increased since 2003 [Di Lorenzo et al., 2008]. We

found a correlation between NPGO and both upwelling and downwelling intensity during the spring season at northern latitudes (Tables 6c,d and 7c,d), which could indicate that increased variance in future NPGO phases could lead to stronger alongshore winds during the spring transition period.

The positive phase of ENSO is a strong indicator of enhanced winter downwelling intensity throughout the study area (Tables 5d and 6d). ENSO has previously been associated with enhanced downwelling intensity throughout the study area [Hsieh et al., 1995; Penland et al., 2010]. Our approach is compares the average ENSO value of the preceding 12 months to a given year's winter downwelling intensity (i.e., the ENSO average for 1986 would be compared to the winter season starting in 1986 and ending in 1987). The effect of climate change on future ENSO conditions is uncertain, but there is a small probability of more El Niño phases in the future [Collins et al., 2005]. A climate experiencing more El Niño conditions would lead to enhanced downwelling during the winter throughout the study area, and therefore affect upper trophic levels the following year due to reduced primary productivity [Ianson and Allen, 2002; Ware and Thomson, 2005].

5: CONCLUSION

We present objective criteria that successfully demarcate the upwelling and downwelling seasons along the northeastern Pacific continental shelf. Summer upwelling is determined by integrating negative AWS occurring over a calendar year. The upwelling season begins when 10% of the total annual negative AWS has been reached and ends when 90% has occurred. Similarly, the winter downwelling season is determined from the percentage of total positive AWS occurring between two consecutive summer seasons. Comparison with an alternative method based on current measurements to determine seasons in our study area (TW96) shows general agreement (Table 4). Our new criteria allow more robust analyses of changes in upwelling (downwelling) behaviour through time by isolating the period of the year where the majority of upwelling (downwelling) favourable winds occurs, and relies on wind data alone, which are much easier to obtain than ocean current data.

Generally, the onset, duration, and intensity of seasons show high interannual variability; on the order of 50 to 100 days for onset and duration, and 5 to 10 Nm-2 per season for upwelling and downwelling intensity (Figure 5). Winter onset occurs earlier and increases in duration and intensity with increasing latitude. The same is true for summer onset, duration, and intensity as latitude decreases.

There were few significant temporal trends in the onset, duration, or intensity of seasons in either NCEP or NARR time series. However, linear regression of the time series derived NARR data (1979-2010) did indicate a significant intensification of summer upwelling with time off the coast near the Oregon-California border and also near the mouth of the Strait of Juan de Fuca. However, these trends were not found in the longer (1948-2010) NCEP time series from nearby locations. Regression analysis of NCEP time series indicated significantly earlier summer onset and shorter summer duration, but these results are likely an artefact of the 1977-1978 PDO regime shift (Table 5; Figure 7). The NCEP analysis therefore indicates that summer upwelling seasons are shorter and have occurred later post-1978 than pre-1978, throughout most of the study area.

Correlation tests between NARR and NCEP time series and PDO, ENSO, and NPGO indicated that 1) few correlations exist for the onset, duration and intensity of most seasons in our study area; 2) the positive phase of the PDO leads to later and shorter upwelling seasons, but not necessarily less total upwelling in the PNW; 3) warm phase ENSO events lead to earlier summer onsets and more intense downwelling throughout the study area; and 4) NPGO has a limited influence on wind regimes north of 38° N. Correlations were also generally stronger with NCEP data because the time series are longer.

In general, our research characterizes a system which has experienced large interannual to interdecadal variability in the onset, duration and intensity of upwelling and downwelling since 1948. The variability of coastal winds swamps

any temporal trend introduced by global climate change, but is linked to large scale climate oscillations. Time series that indicate changes in alongshore winds along the northeastern Pacific continental shelf but are too short to resolve climate oscillations should be treated with caution.

APPENDICES

Appendix A – Auxiliary Material

Introduction

The Auxiliary Information contains two tables and 22 figures.

1. Table A.1
We applied screening criteria in which daily observational data were omitted if less than 7 hourly measurements were recorded. This analysis drastically reduced the number of days which could be used for our analysis. A summary of the number of gaps, and their distribution amongst the observation locations is provided.

2. Table A.2
The median and variance of summer and winter onset, duration, and (upwelling and downwelling) intensity for all NARR and NCEP stations, between 1979 and 2010, and 1948 and 2010, respectively.

3. Figure A.1
Sensitivity of the choices of summer onset at NARR location A between 1979 to 2010 to 12 different choices of Running Average (RA). For each choice of RA, a cut-off percentage (COP) of 2% (green), 10% (red), and 18% (blue) are shown.

4. Figure A.2
Sensitivity of the choices of summer onset at NARR location K between 1979 to 2010 to 12 different choices of Running Average (RA). For each choice of RA, a cut-off percentage (COP) of 2% (green), 10% (red), and 18% (blue) are shown.

5. Figure A.3
Sensitivity of the choices of summer onset at NARR location W between 1979 to 2010 to 12 different choices of Running Average (RA). For each choice of RA, a cut-off percentage (COP) of 2% (green), 10% (red), and 18% (blue) are shown.

6. Figure A.4
Sensitivity of the choices of summer onset at NARR location A between 1979 to 2010 to 3 different choices of Running Average (RA) and 5 choices Cut-off Percentage (COP).

7. Figure A.5

Sensitivity of the choices of summer onset at NARR location K between 1979 to 2010 to 3 different choices of Running Average (RA) and 5 choices Cut-off Percentage (COP).

8. Figure A.6
Sensitivity of the choices of summer onset at NARR location K betwen 1979 to 2010 to 3 different choices of Running Average (RA) and 5 choices Cut-off Percentage (COP).

9. Figure A.7
Time series of summer onset at NARR locations A through N between 1979 and 2010.

10. Figure A.8
Time series of summer onset at NARR locations O through Z between 1979 and 2010.

11. Figure A.9
Time series of winter onset at NARR locations A through N between 1979 and 2010.

12. Figure A.10
Time series of winter onset at NARR locations O through Z between 1979 and 2010.

13. Figure A.11
Time series of summer length at NARR locations A through N between 1979 and 2010.

14. Figure A.12
Time series of summer length at NARR locations O through Z between 1979 and 2010.

15. Figure A.13
Time series of winter length at NARR locations A through N between 1979 and 2010.

16. Figure A.14
Time series of winter length at NARR locations O through Z between 1979 and 2010.

17. Figure A.15
Time series of summer upwelling intensity at NARR locations A through N between 1979 and 2010.

18. Figure A.16

Time series of summer upwelling intensity at NARR locations O through Z between 1979 and 2010. Note the change in scale from Figure 15.

19. Figure A.17
Time series of winter downwelling intensity at NARR locations A through N between 1979 and 2010.

20. Figure A.18
Time series of winter downwelling intensity at NARR locations O through Z between 1979 and 2010.

21. Figure A.19
Dendrogram of clustering results for the onset of all seasons for all NARR locations.

22. Figure A.20
Dendrogram of clustering results for the length of all seasons for all NARR locations.

23. Figure A.21
Dendrogram of clustering results for the upwelling intensity for all NARR locations.

24. Figure A.22
Dendrogram of clustering results for the downwelling intensity for all NARR locations.

Table A.1

Station	Maximum Gap (days)	Average Gap (days)	Number of Gaps	Total Days Missing
I	177	48.96	25	1224
II	333	34.97	39	1364
III	320	20.97	32	671
IV	229	34.93	42	1467
V	518	45.35	52	2358
VI	12	2.76	17	47
VII	231	54.73	26	1423
VIII	1712	72.83	53	3860
IX	365	87.30	23	2008
X	99	8.32	19	158
XI	129	5.97	175	1045
XII	123	5.08	145	736

Table A.2

	Location	Summer Start (Julian Day)		Winter Start (Julian Day)		Summer Length (Days)		Winter Length (Days)		Summer Upwelling Intensity (Nm^{-2})		Winter Downwelling Intensity (Nm^{-2})	
		Median	SD	Median	SD	Median	SD	Median	SD	Median	SD	Median	SD
NARR Locations	Z	153	44	300	28	88	55	159	41	-3.14	1.41	10.82	2.85
	Y	154	44	296	23	83	51	160	39	-2.83	1.29	12.57	2.95
	X	153	27	303	16	87	32	150	24	-5.04	1.62	14.37	3.08
	W	149	24	304	15	93	31	147	25	-4.50	1.46	12.41	2.53
	V	145	25	304	17	104	30	141	26	-6.10	1.65	12.80	2.94
	U	135	25	309	19	112	31	138	26	-4.05	1.12	7.90	1.81
	T	127	22	309	20	123	27	125	25	-3.20	0.85	4.43	1.02
	S	140	25	302	15	95	32	147	23	-1.94	0.65	7.91	1.49
	R	136	23	307	17	114	30	136	23	-2.95	0.92	6.51	1.43
	Q	131	20	309	16	116	26	127	23	-3.62	0.81	5.11	1.19
	P	138	21	306	16	116	31	135	22	-3.07	0.80	5.80	1.44
	O	136	21	307	16	120	30	134	22	-3.80	0.98	6.76	1.86
	N	139	24	309	15	115	32	126	25	-4.87	1.14	6.16	2.07
	M	137	23	311	15	121	31	123	26	-5.71	1.25	5.98	2.14
	L	138	24	311	15	122	31	119	27	-5.77	1.28	6.10	2.36
	K	138	24	316	16	130	32	116	27	-7.47	1.59	6.83	2.70
	J	134	25	317	14	131	31	110	27	-7.77	1.54	6.48	2.71
	I	128	25	324	18	138	27	102	31	-12.30	2.69	6.77	3.19
	H	115	25	329	24	154	28	87	29	-11.15	1.66	4.27	2.16
	G	108	28	331	24	162	33	81	31	-11.46	2.23	4.67	2.44
	F	107	28	333	24	165	35	79	31	-13.01	2.20	4.54	2.38
	E	103	27	335	23	176	33	71	32	-19.94	2.50	4.21	2.02
	D	92	25	348	25	193	32	44	30	-20.65	2.40	2.58	1.43
	C	91	22	351	24	192	30	42	26	-20.06	2.54	2.29	1.36
	B	82	19	362	22	204	25	25	22	-19.38	2.88	0.98	0.89
	A	80	19	367	25	211	24	23	16	-15.18	2.39	0.75	0.80
NCEP Locations	ζ	140	34	302	20	107	39	138	29	-2.12	0.64	5.61	1.51
	ε	139	25	306	15	110	28	135	23	-3.18	0.75	6.21	1.50
	δ	145	21	313	16	116	25	126	24	-4.83	0.97	7.19	1.89
	γ	133	23	320	18	132	26	102	26	-7.65	1.32	5.78	1.95
	β	112	23	332	28	158	25	76	31	-11.74	1.47	4.19	1.91
	α	80	22	359	29	207	31	26	22	-13.34	1.96	0.79	0.83

Figure A.1

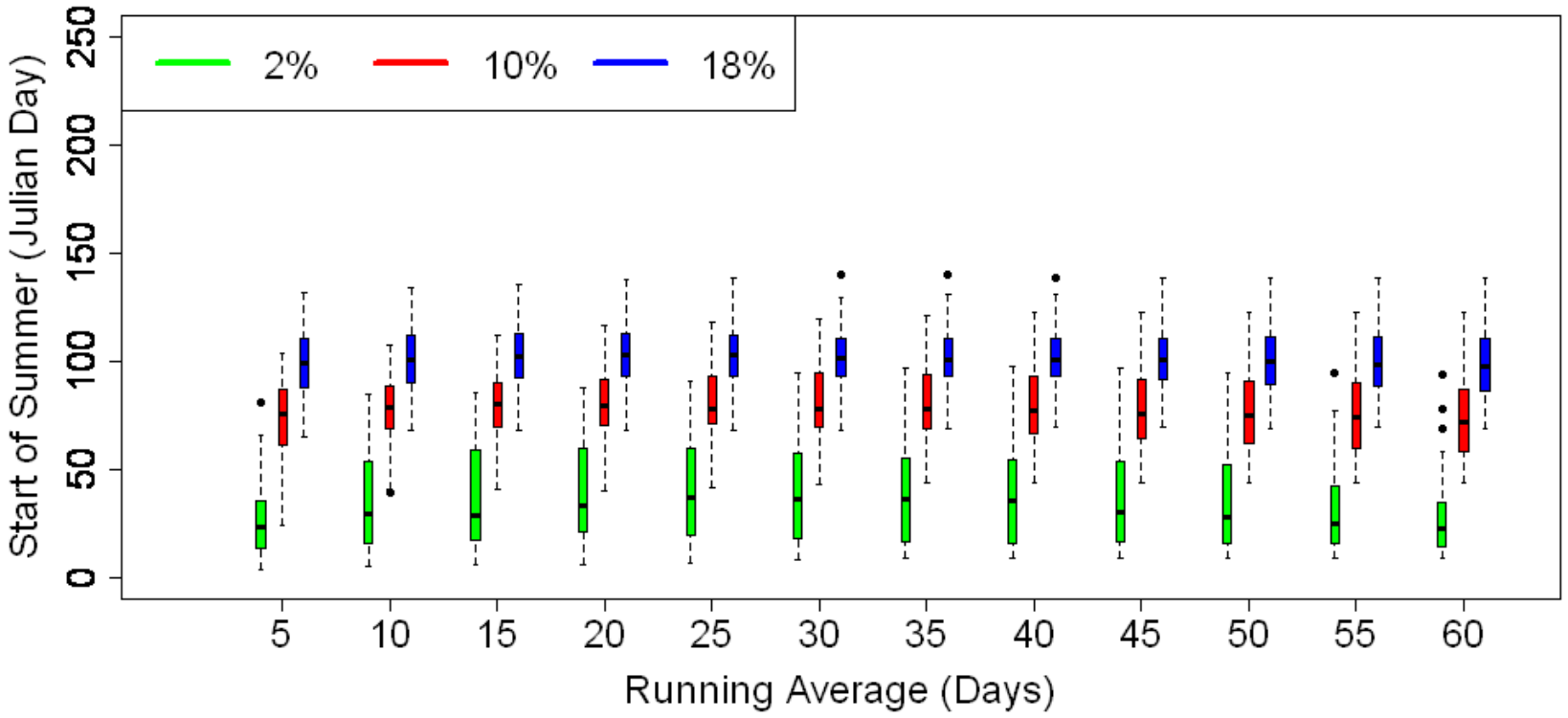
2%
10%
18%
Start of Summer (Julian Day)
0
50
100
150
200
250
5
10
15
20
25
30
35
40
45
50
55
60
Running Average (Days)

Figure A.2

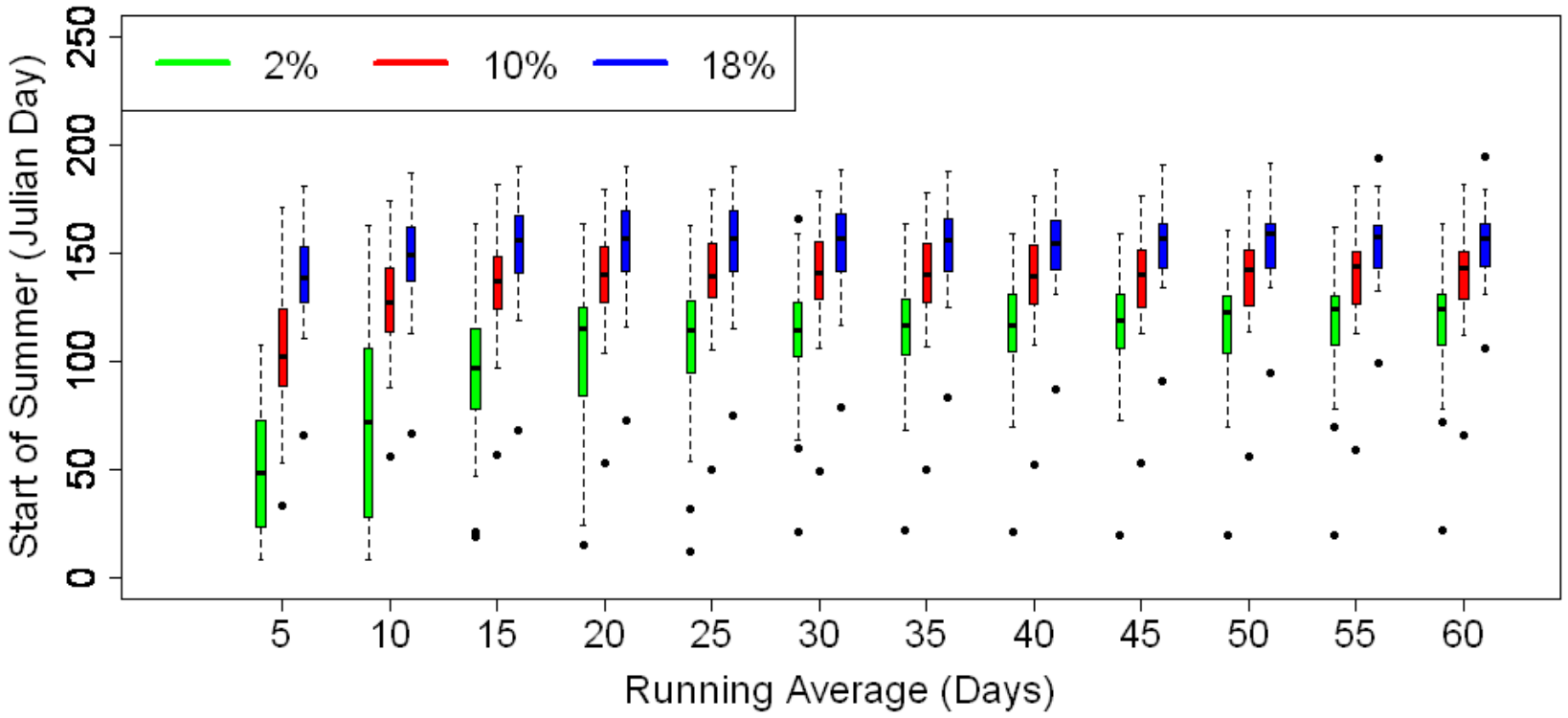
2%
10%
18%
Start of Summer (Julian Day)
0
50
100
150
200
250
5
10
15
20
25
30
35
40
45
50
55
60
Running Average (Days)

Figure A.3

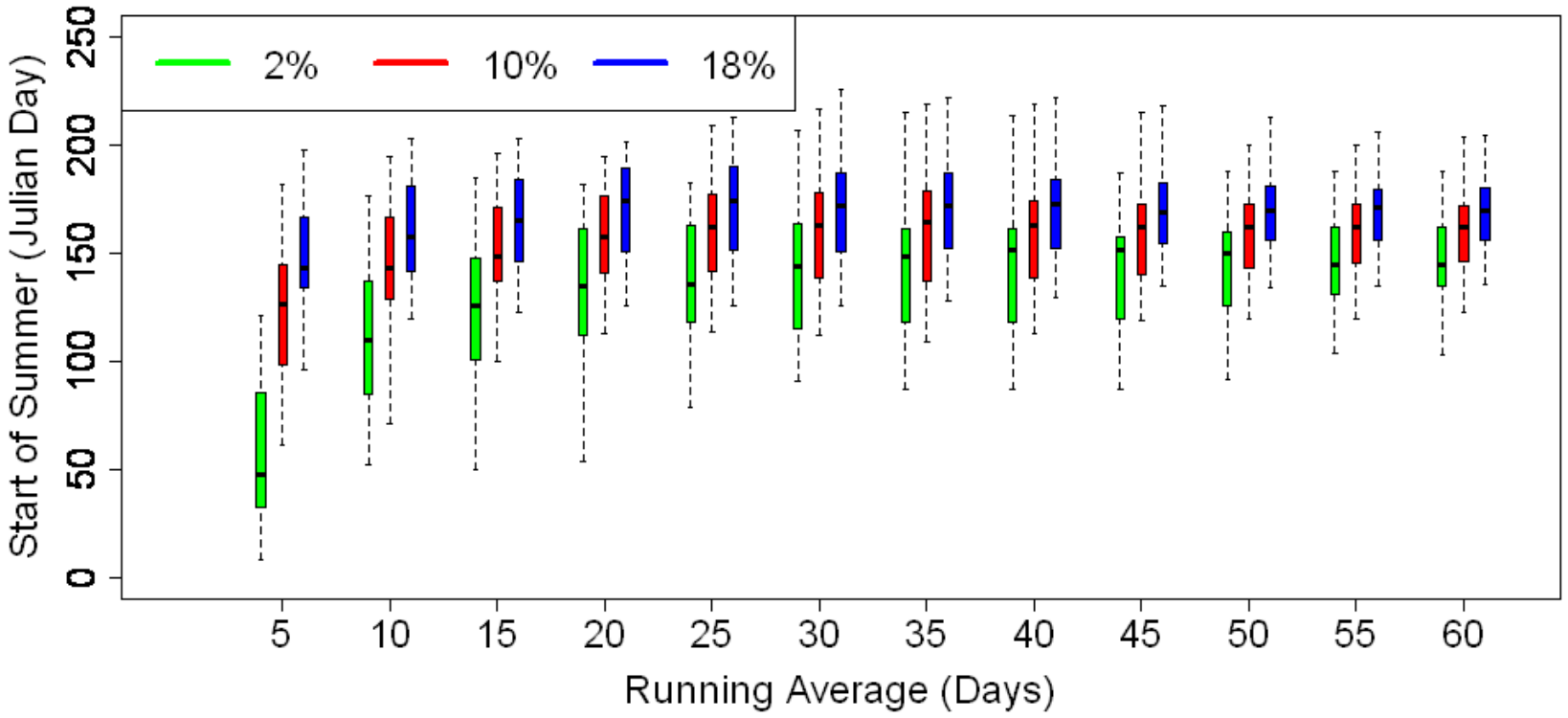
2%
10%
18%
Start of Summer (Julian Day)
0
50
100
150
200
250
5
10
15
20
25
30
35
40
45
50
55
60
Running Average (Days)

Figure A.4

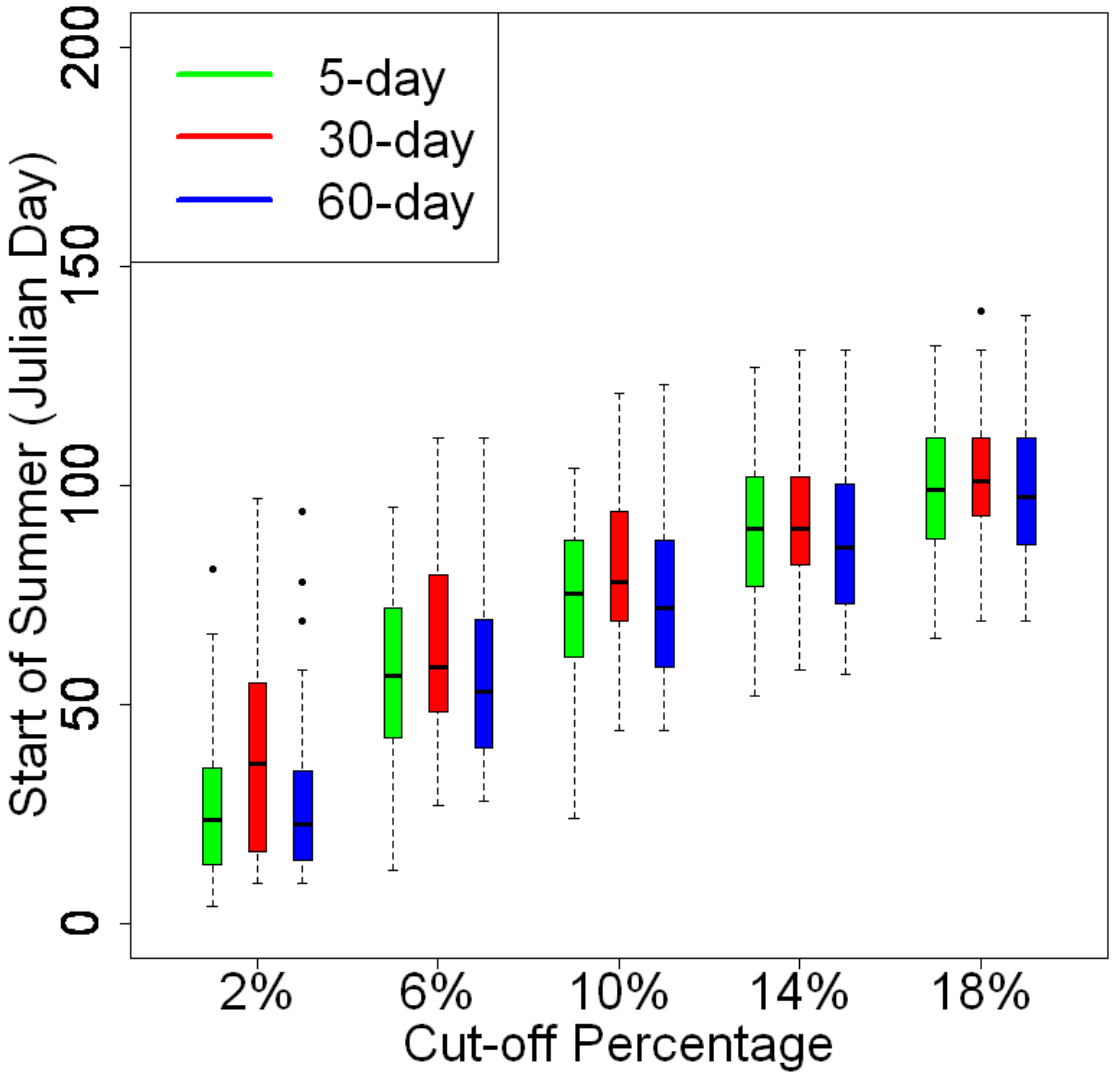
5-day
30-day
60-day
Start of Summer (Julian Day)
0
50
100
150
200
2%
6%
10%
14%
18%
Cut-off Percentage

Figure A.5

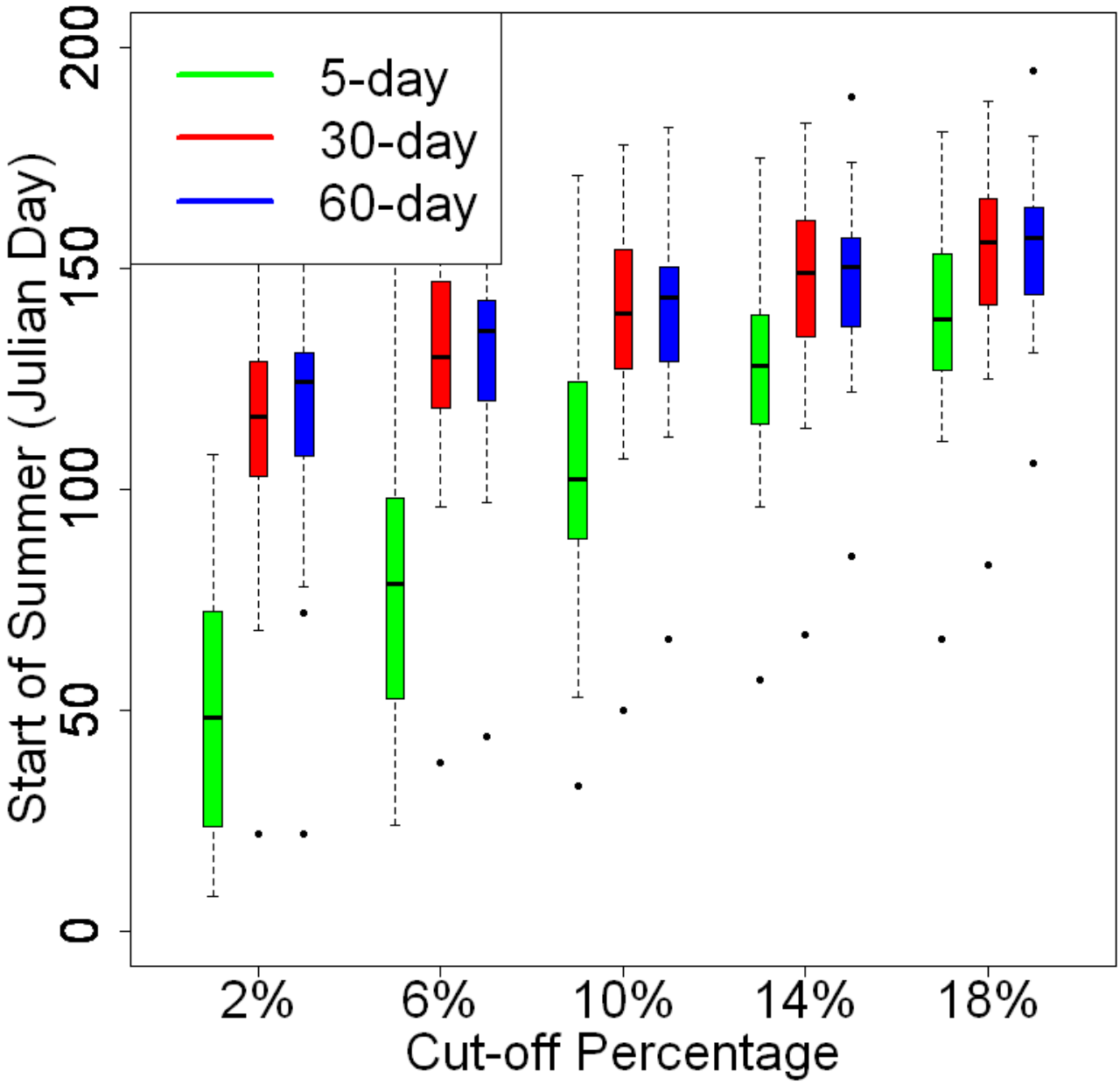
5-day
30-day
60-day
Start of Summer (Julian Day)
0
50
100
150
200
2%
6%
10%
14%
18%
Cut-off Percentage

Figure A.6

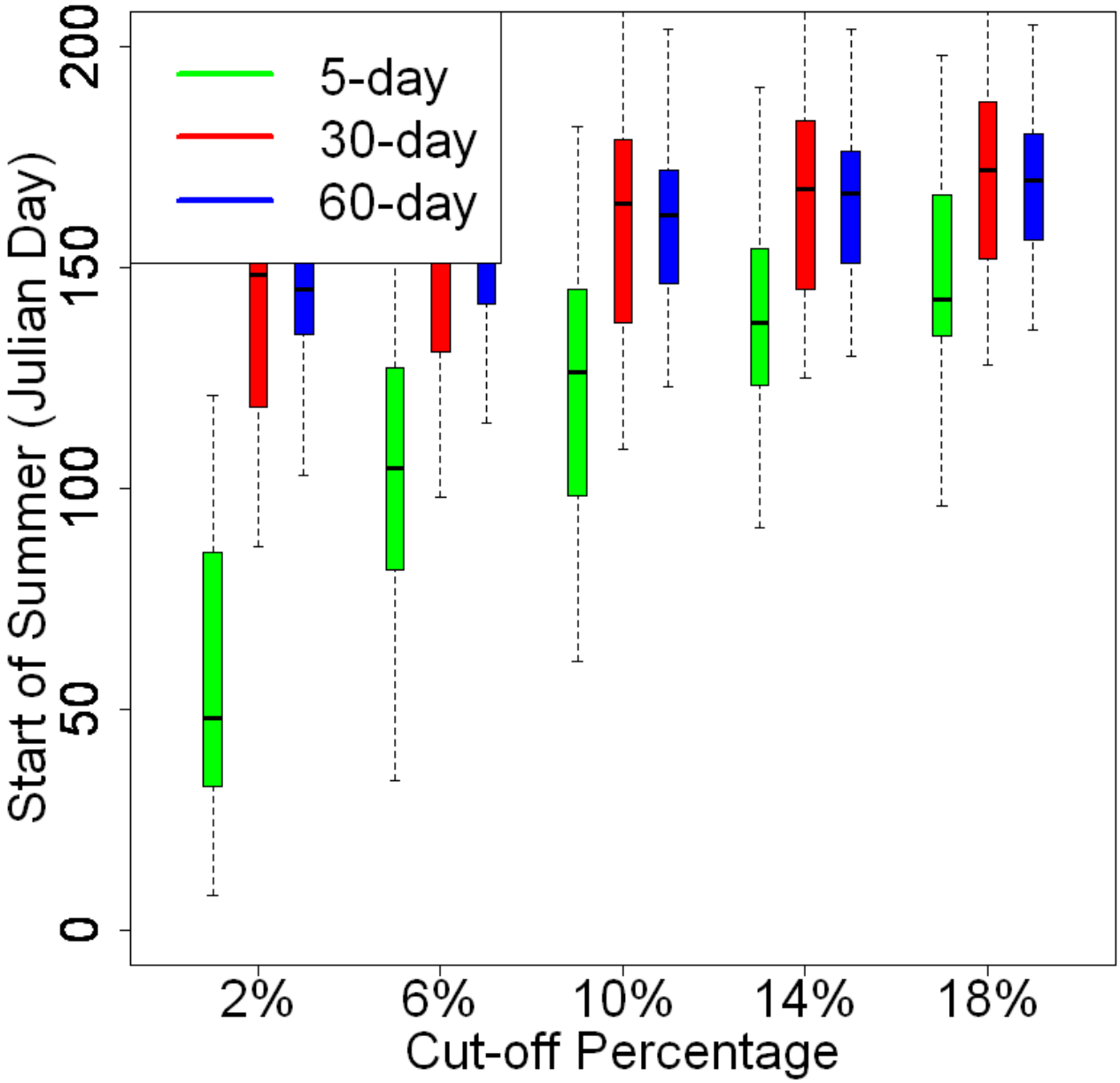
5-day
30-day
60-day
Start of Summer (Julian Day)
0
50
100
150
200
2%
6%
10%
14%
18%
Cut-off Percentage

Figure A.7

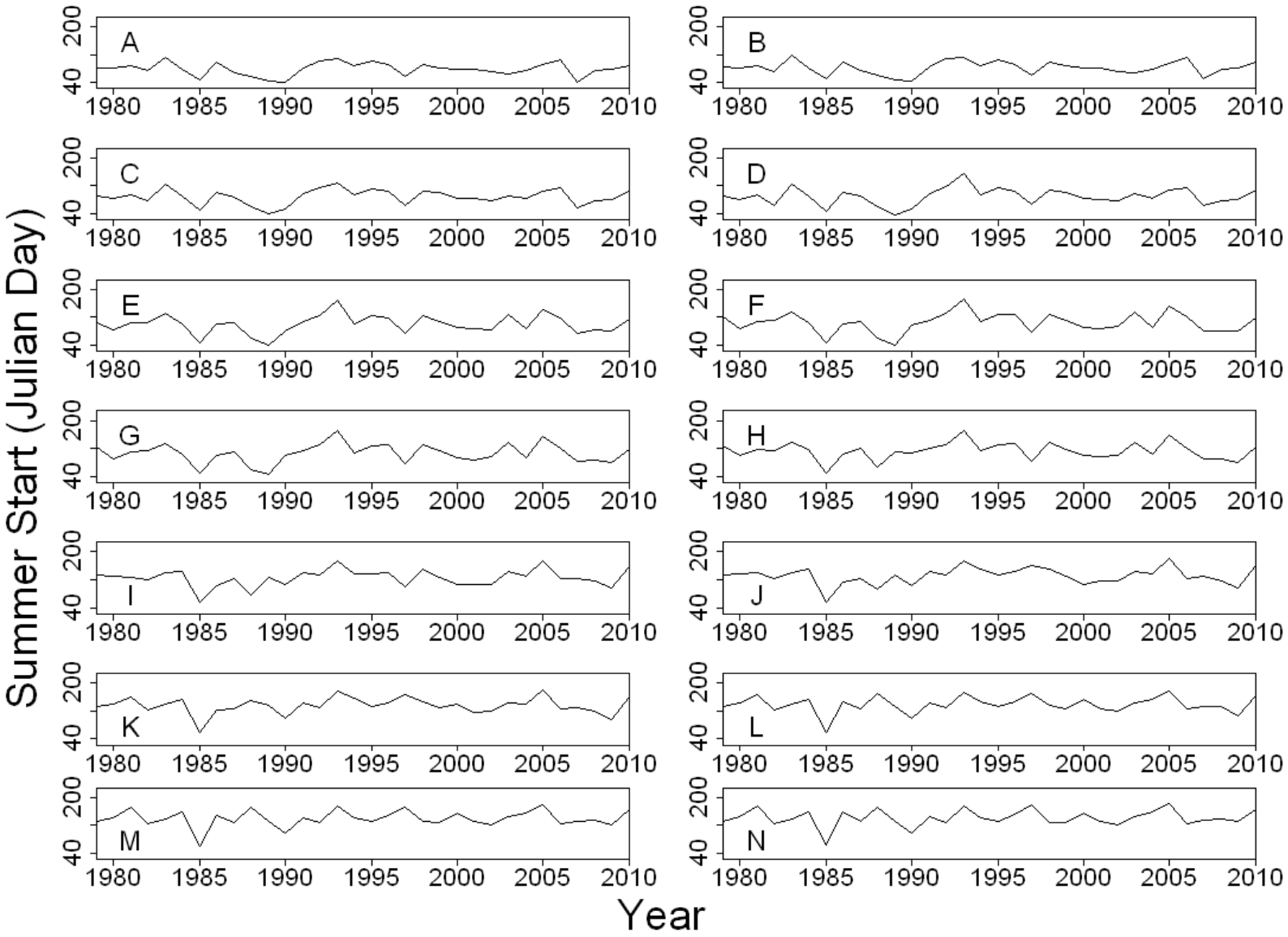
Summer Start (Julian Day)
Year
A
B
C
D
E
F
G
H
I
J
K
L
M
N
40
200
1980
1985
1990
1995
2000
2005
2010

Figure A.8

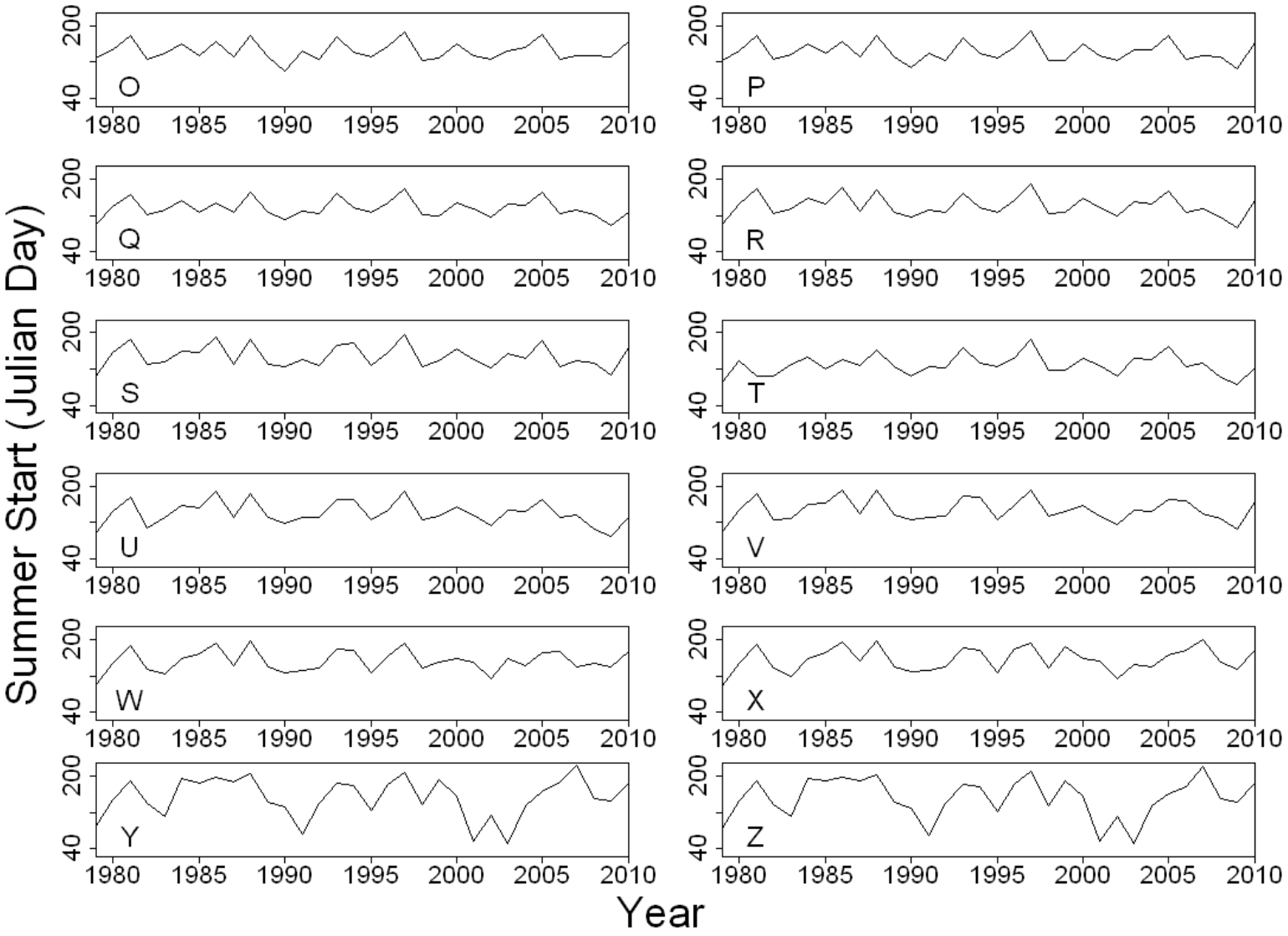
Summer Start (Julian Day)
Year
O
P
Q
R
S
T
U
V
W
X
Y
Z
40
200
1980
1985
1990
1995
2000
2005
2010

Figure A.9

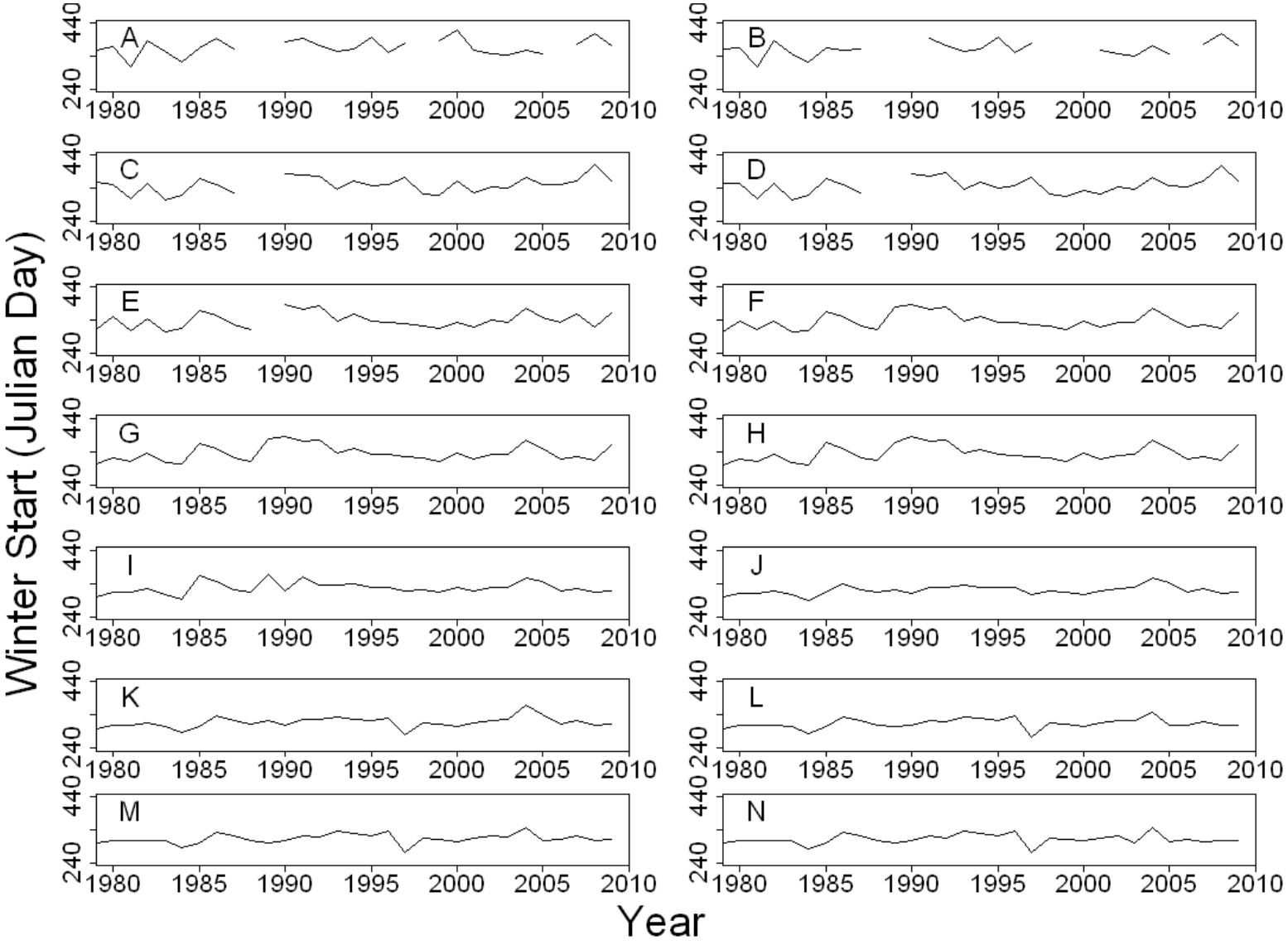
Winter Start (Julian Day)
Year
A
B
C
D
E
F
G
H
I
J
K
L
M
N
240
440
1980
1985
1990
1995
2000
2005
2010

Figure A.10

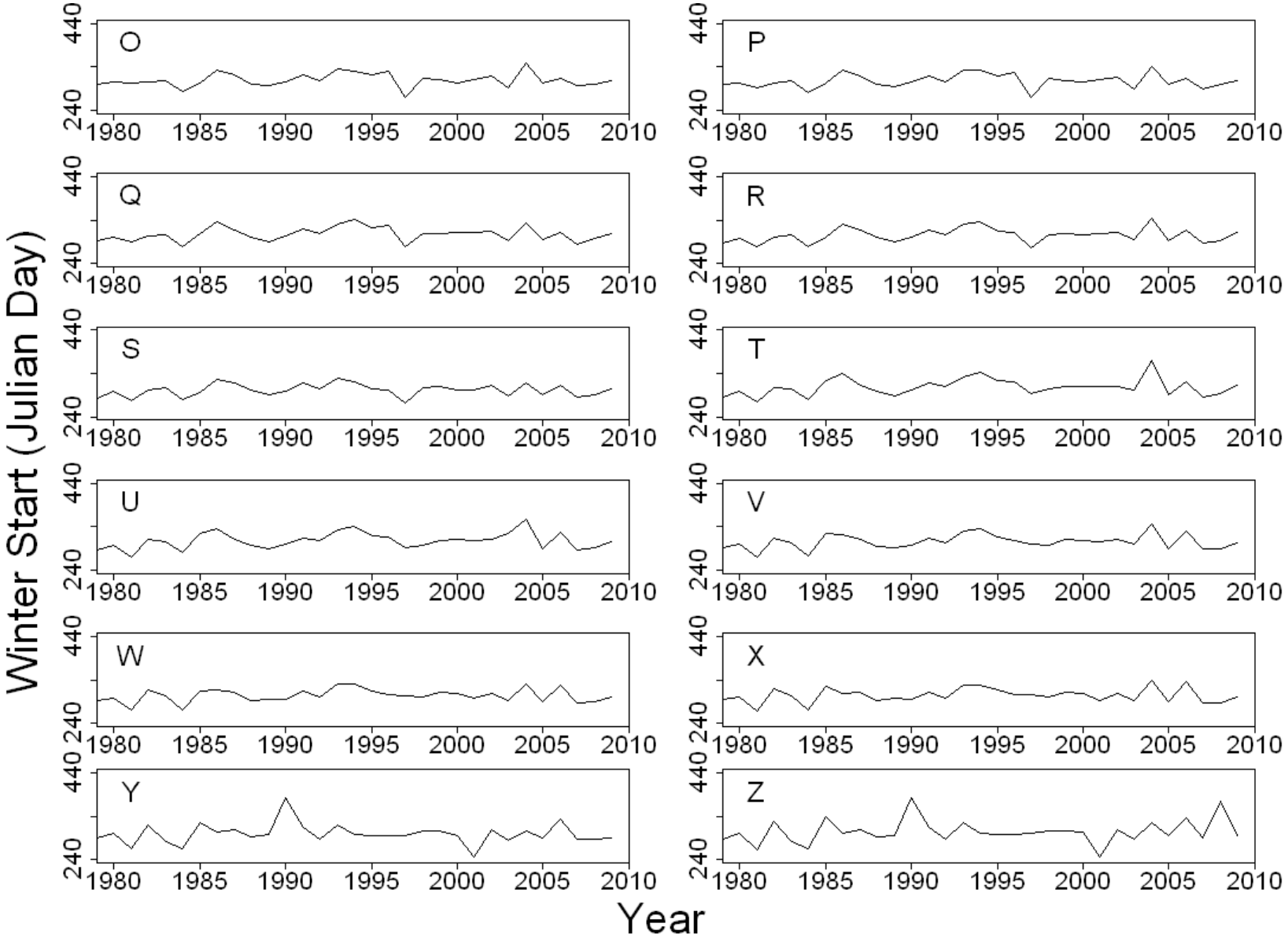
Winter Start (Julian Day)
Year
O
P
Q
R
S
T
U
V
W
X
Y
Z
240
440
1980
1985
1990
1995
2000
2005
2010

Figure A.11

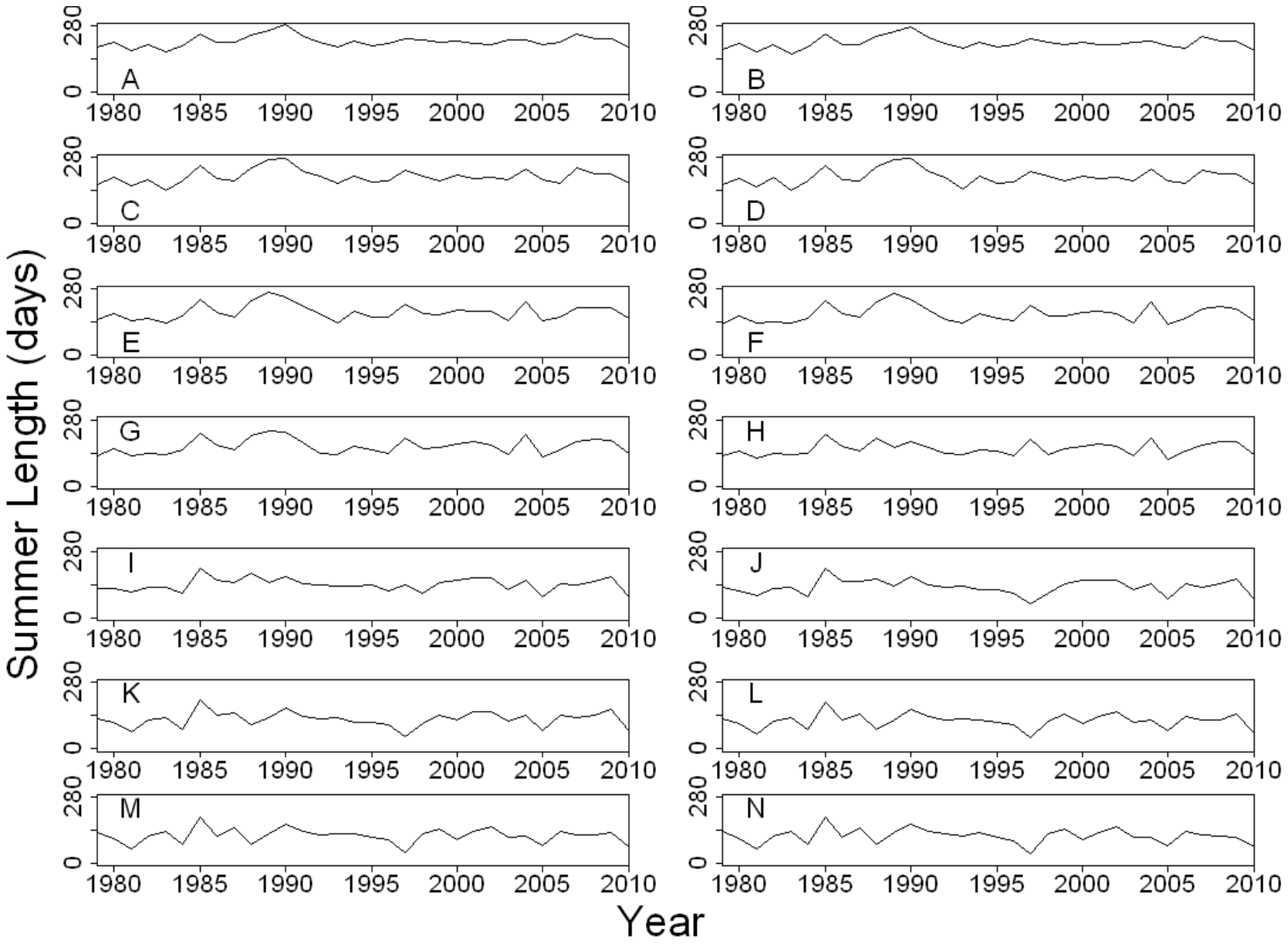
Summer Length (days)
Year
A
B
C
D
E
F
G
H
I
J
K
L
M
N
0
280
1980
1985
1990
1995
2000
2005
2010

Figure A.12

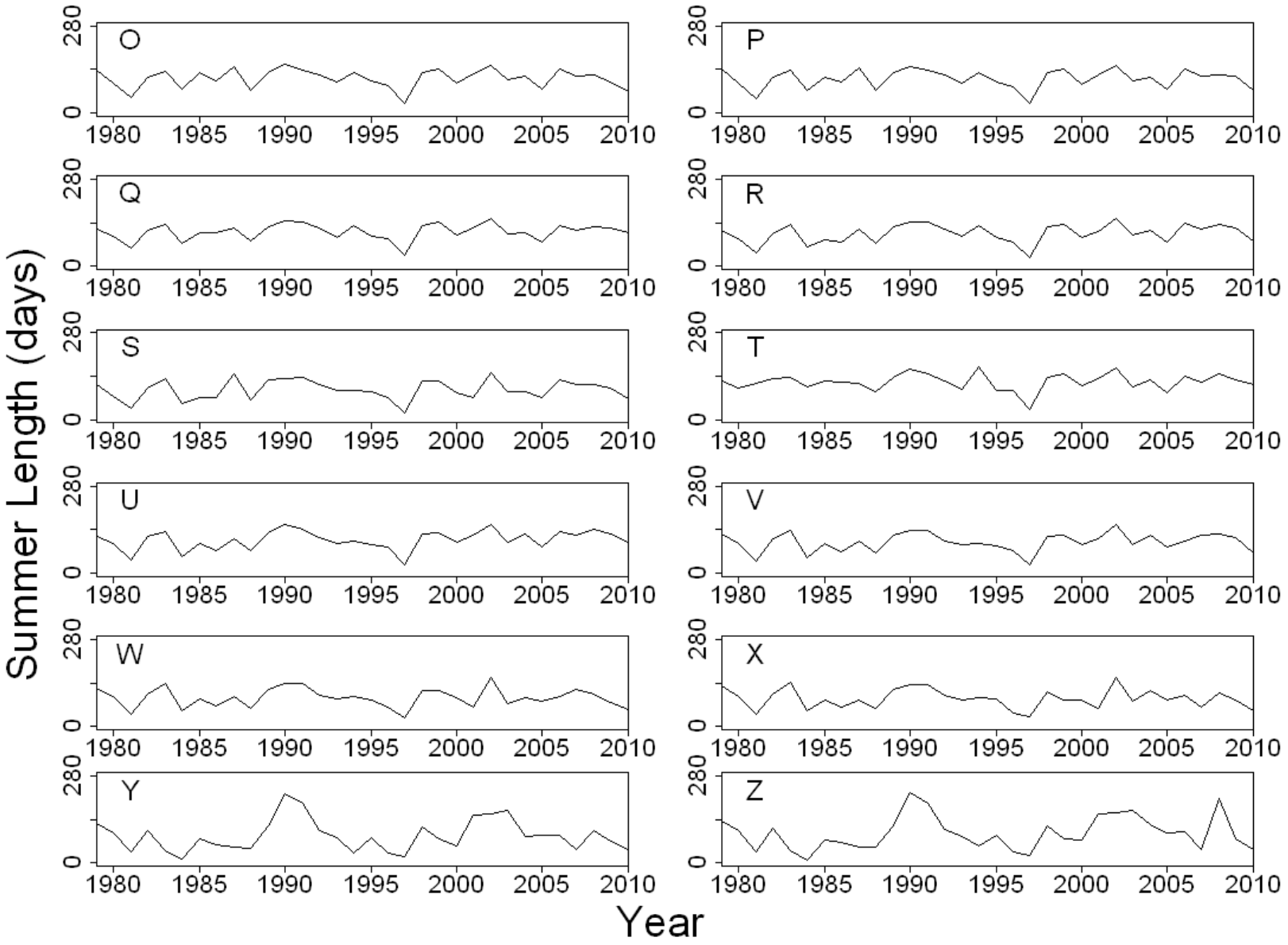
Summer Length (days)
Year
O
P
Q
R
S
T
U
V
W
X
Y
Z
0
280
1980
1985
1990
1995
2000
2005
2010

Figure A.13

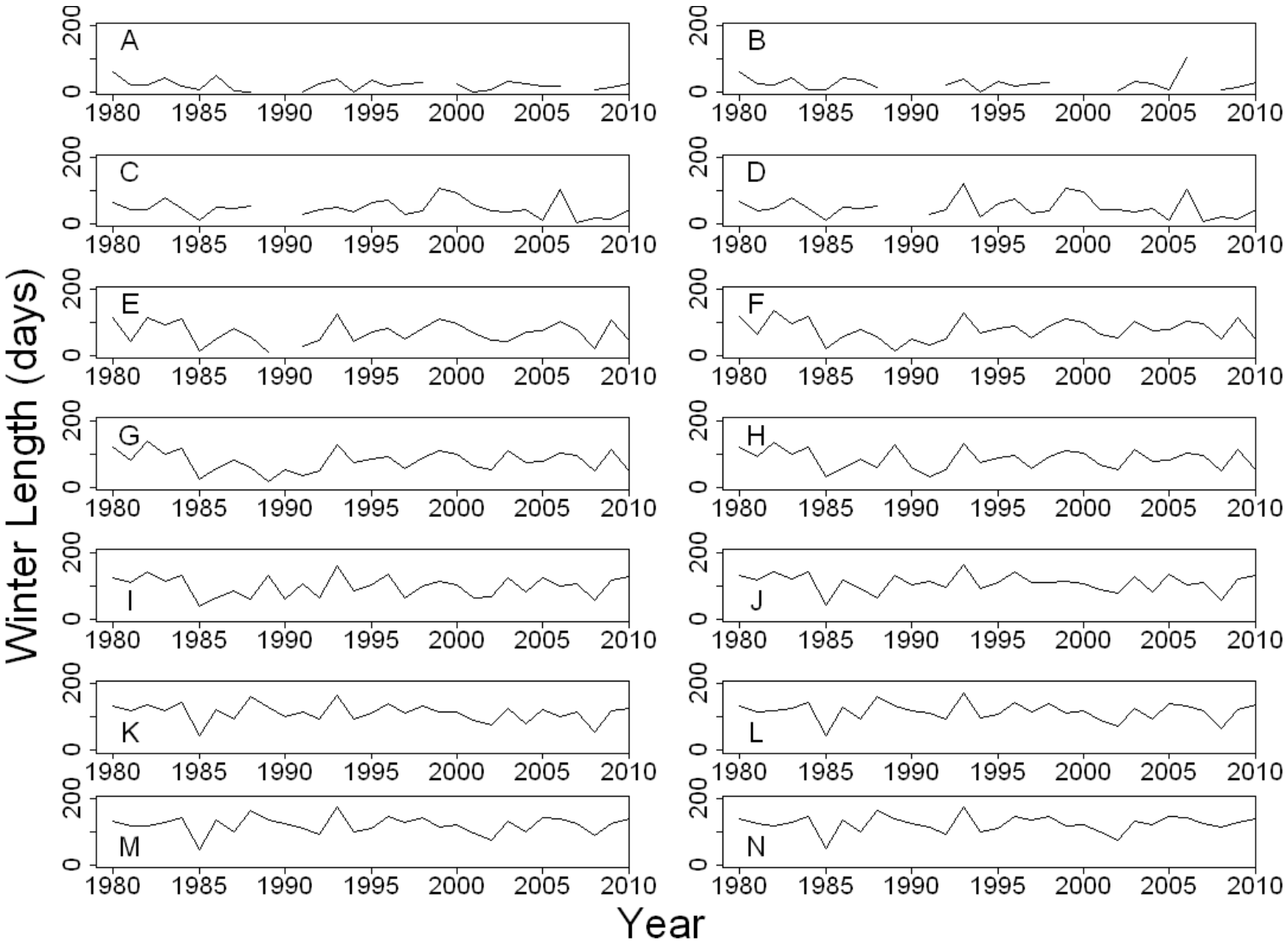
Winter Length (days)
Year
A
B
C
D
E
F
G
H
I
J
K
L
M
N
0
200
1980
1985
1990
1995
2000
2005
2010

Figure A.14

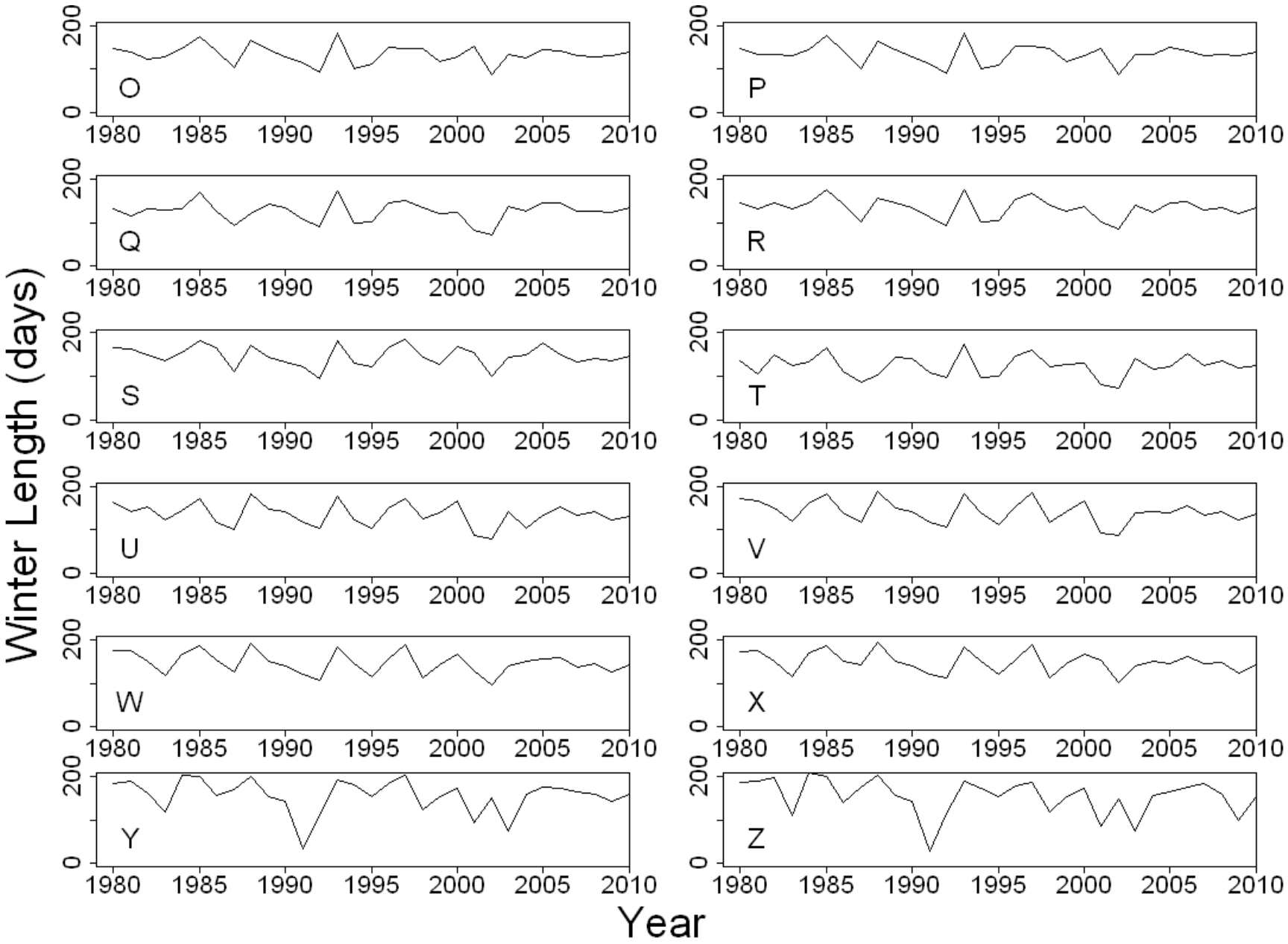
Winter Length (days)
Year
O
P
Q
R
S
T
U
V
W
X
Y
Z
0
200
1980
1985
1990
1995
2000
2005
2010

Figure A.15

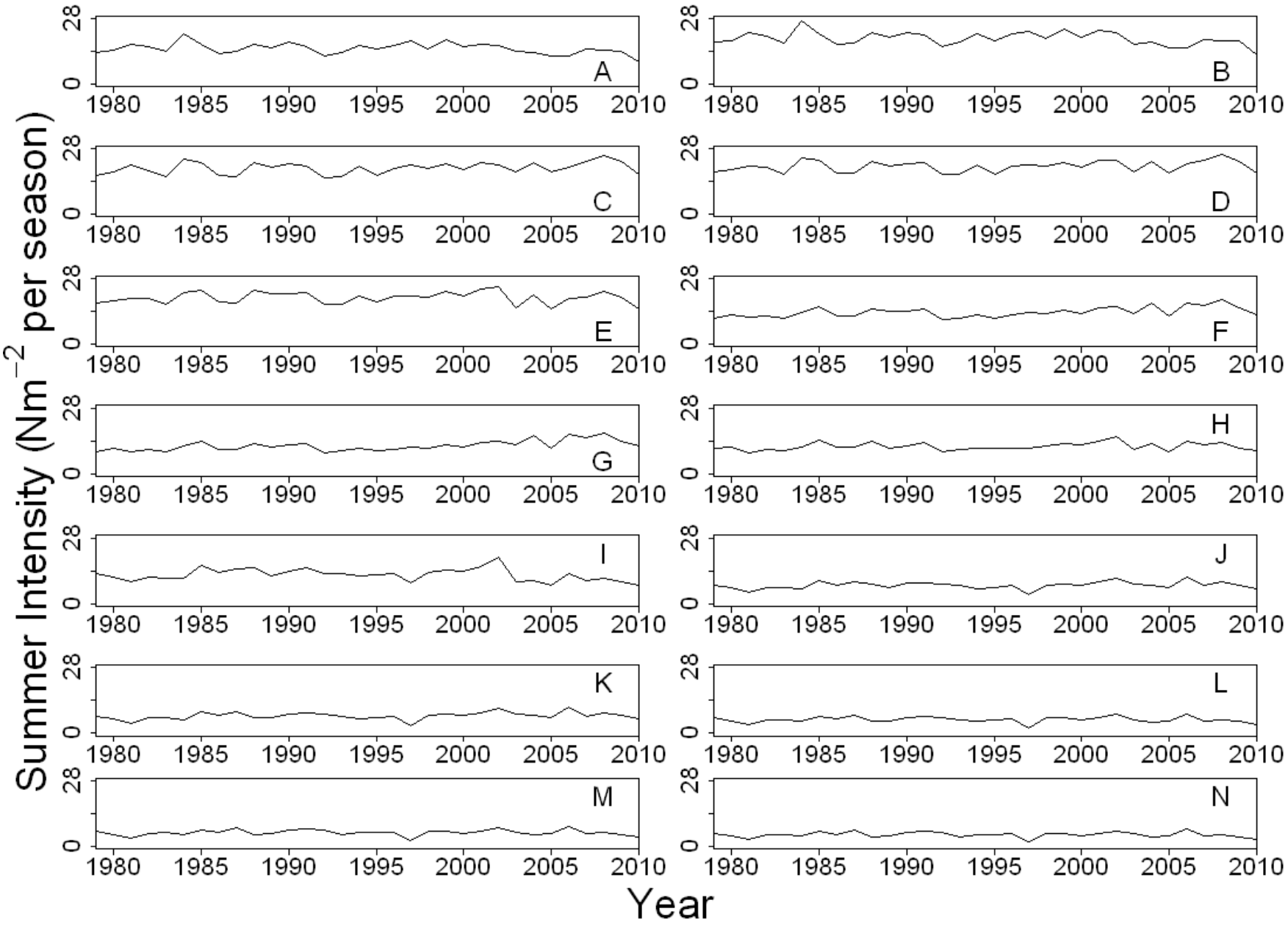
Summer Intensity (Nm^{-2} per season)
Year
A
B
C
D
E
F
G
H
I
J
K
L
M
N
0
28
1980
1985
1990
1995
2000
2005
2010

Figure A.16

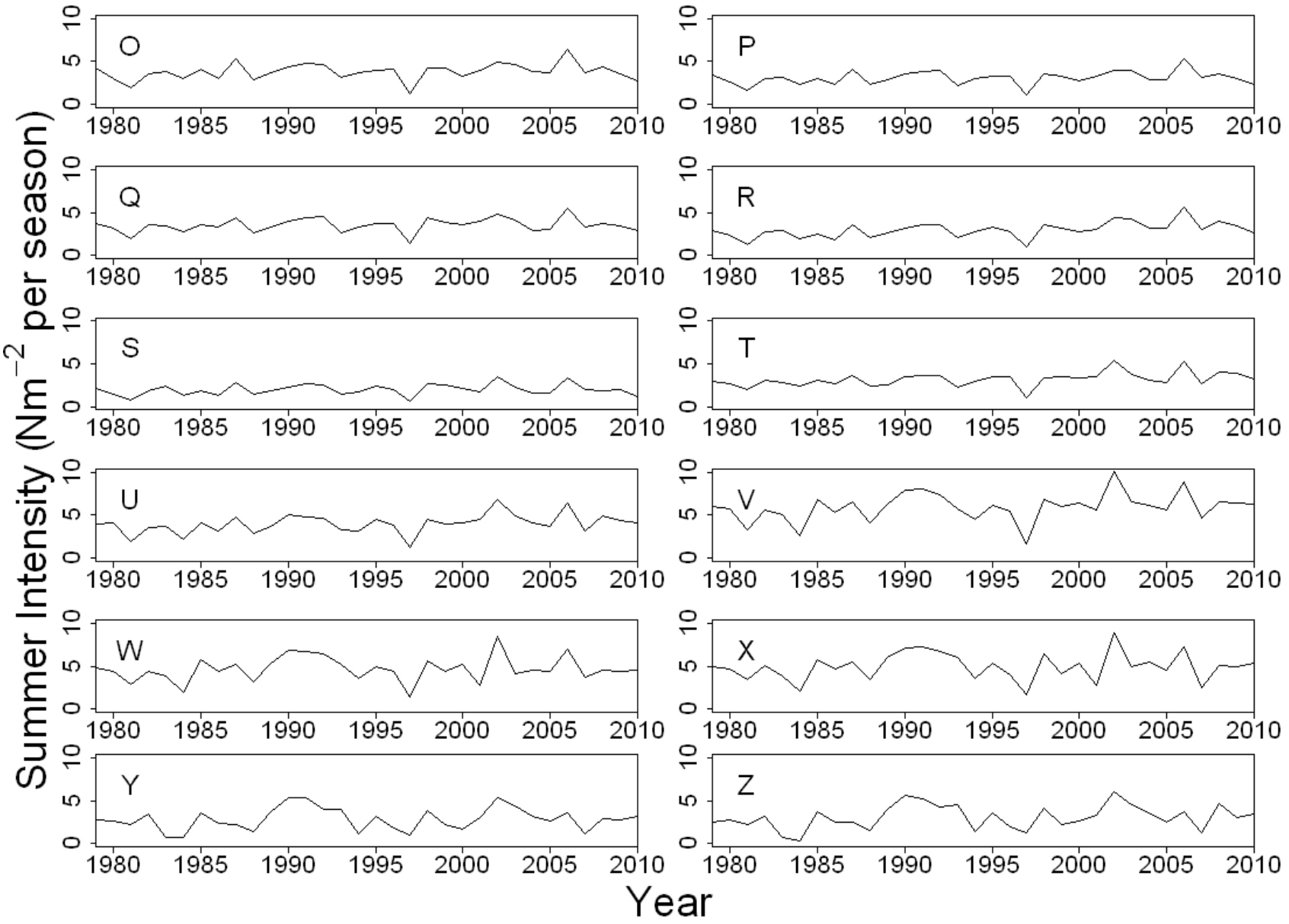
O
P
Q
R
S
T
U
V
W
X
Y
Z
0
5
10
1980
1985
1990
1995
2000
2005
2010
Summer Intensity (Nm^{-2} per season)
Year

Figure A.17

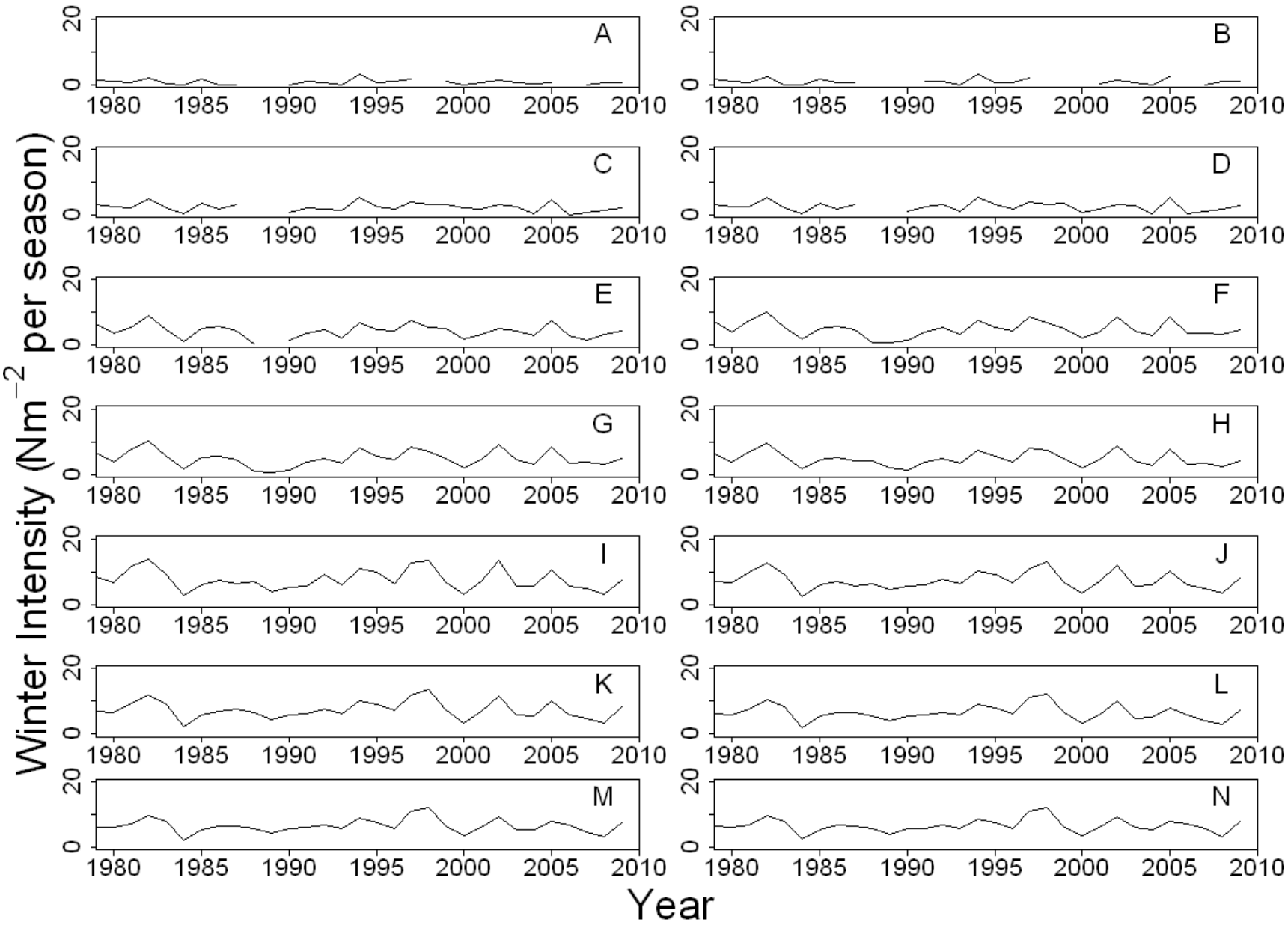
A
B
C
D
E
F
G
H
I
J
K
L
M
N
0
20
1980
1985
1990
1995
2000
2005
2010
Winter Intensity (Nm^{-2} per season)
Year

Figure A.18

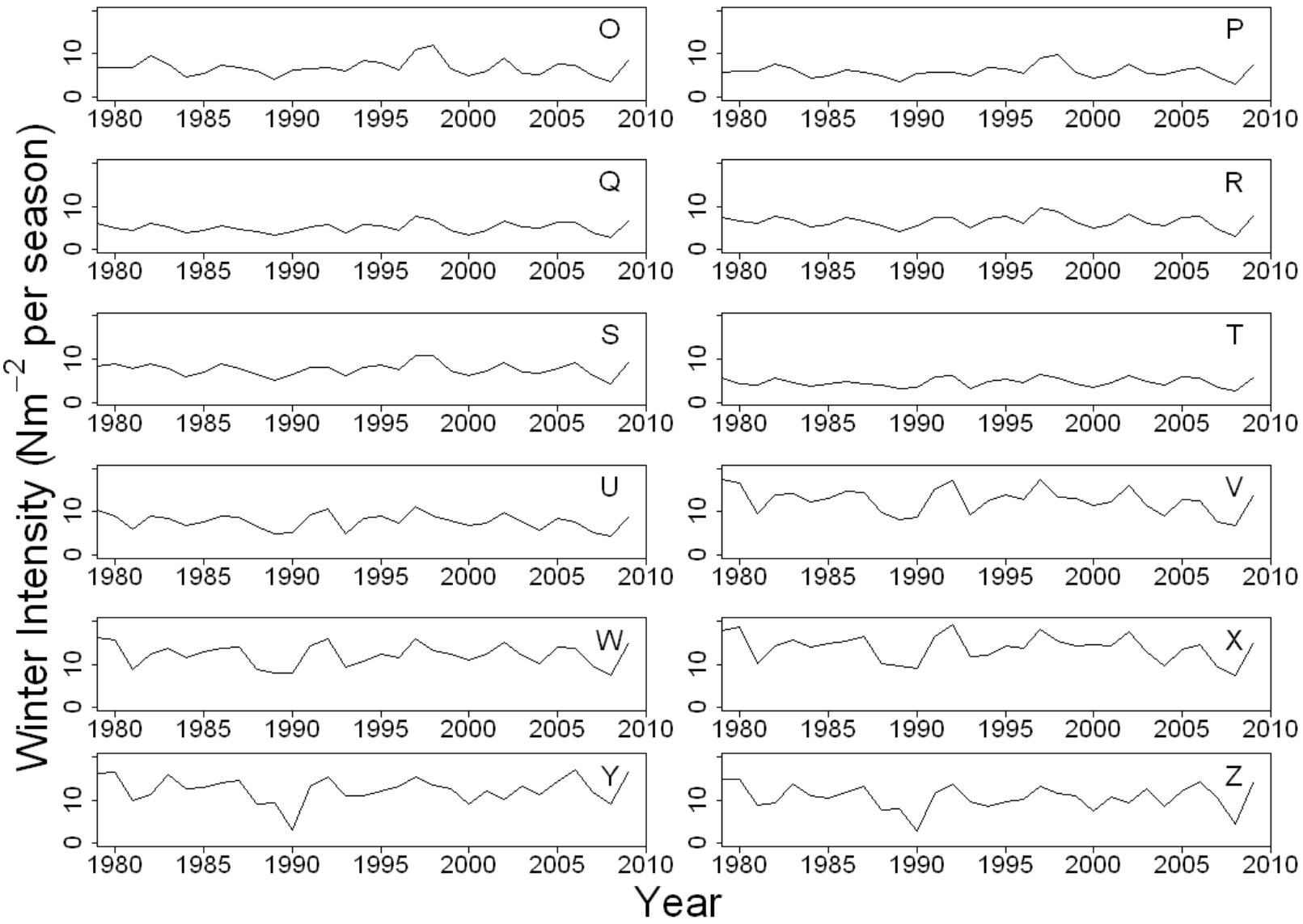
O
P
Q
R
S
T
U
V
W
X
Y
Z
0
10
1980
1985
1990
1995
2000
2005
2010
Winter Intensity (Nm^{-2} per season)
Year

Figure A.19

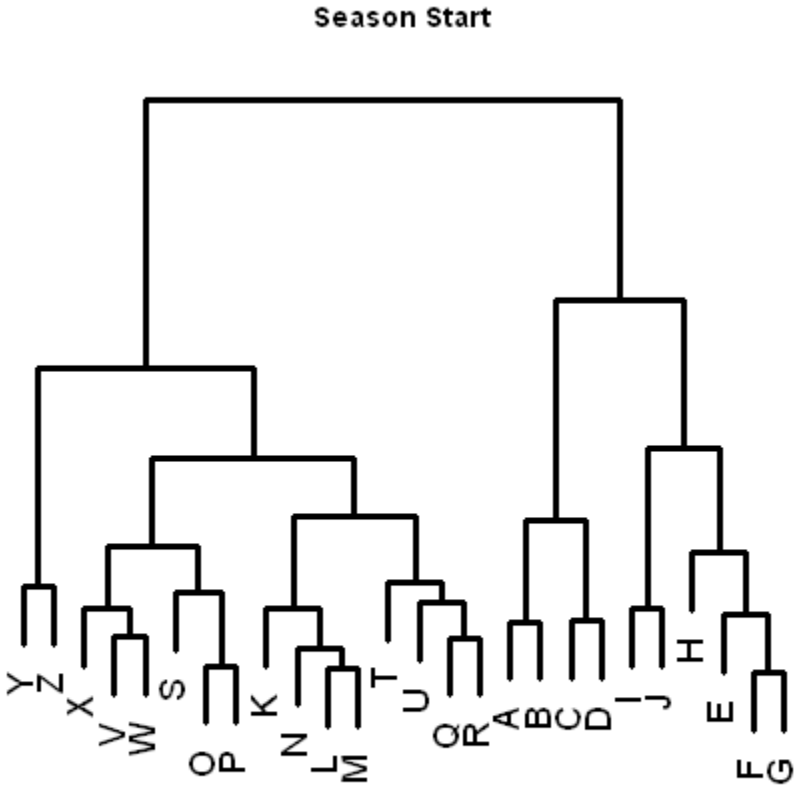

Figure A.20

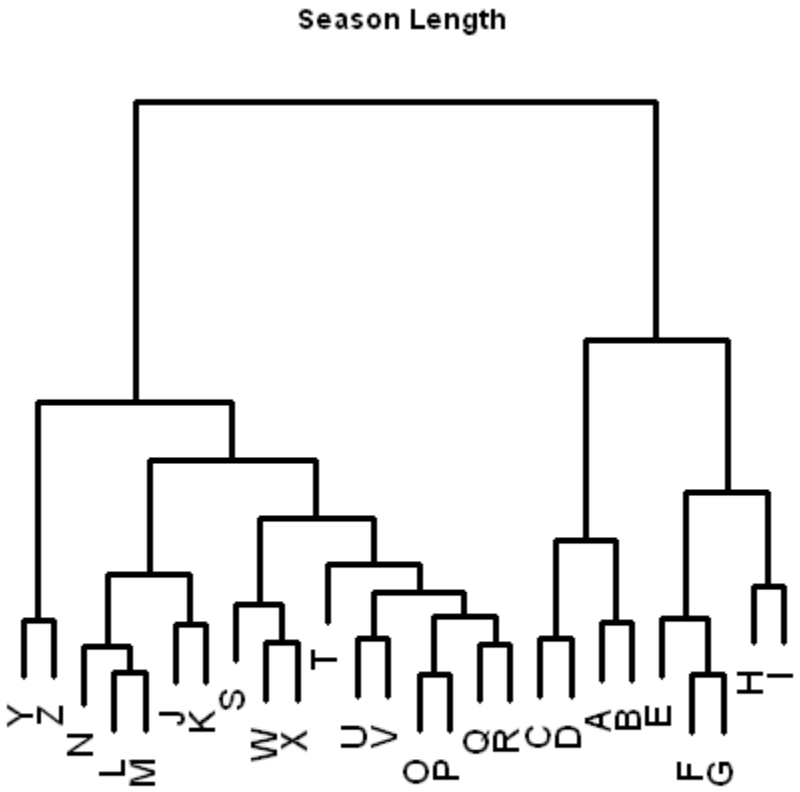

Figure A.21

Upwelling Intensity

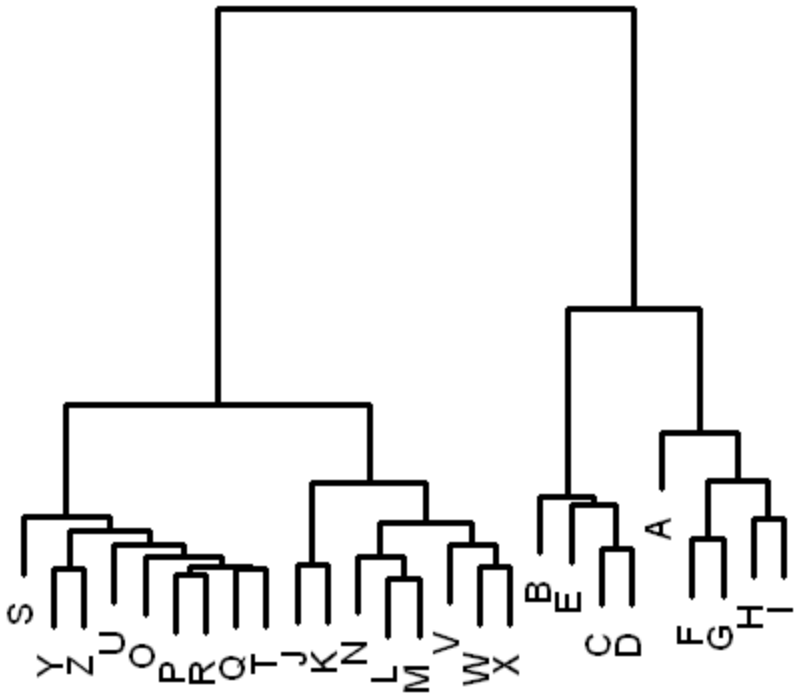

Figure A.22

Downwelling Intensity

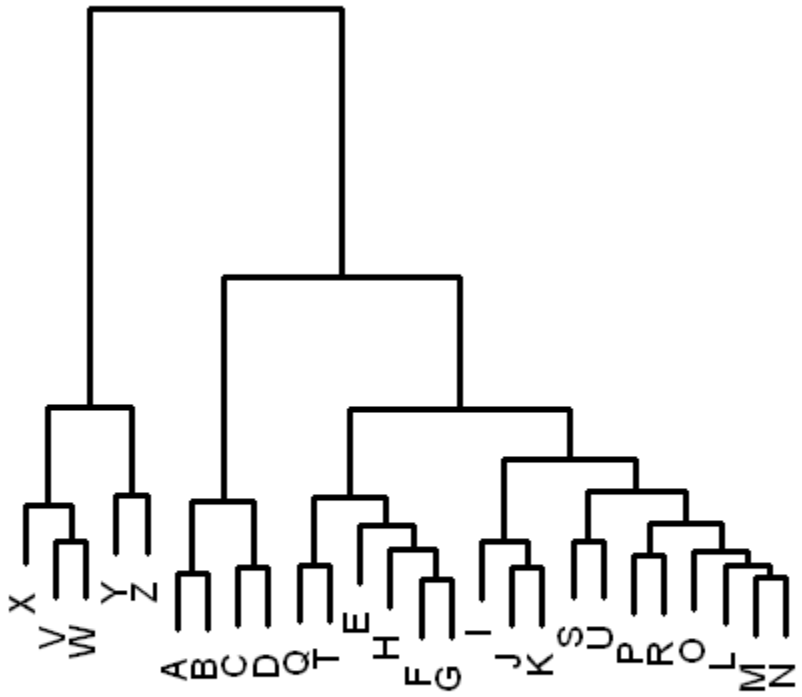

REFERENCE LIST

Auad, G., A. Miller, and E. Di Lorenzo (2006), Long-term forecast of oceanic conditions off California and their biological implications, *J. Geophys. Res., 111*, C09008, doi:10.1029/2005JC003219.

Bakun, A. (1990), Global Climate Change and Intensification of Coastal Ocean Upwelling, *Science, 247*, 198-201.

Bakun, A., D.B. Field, A. Redondo-Rodriguez, and S.J. Weeks (2010), Greenhouse gas, upwelling-favorable winds, and the future of coastal ocean upwelling ecosystems, *Global Change Biology, 16*, 1213-1228, doi:10.1111/j.1365-2486.2009.02094.x.

Barth, J.A., B.A. Menge, J. Lubchenco, F. Chan, J.M. Bane, A.R. Kirincich, M.A. McManus, K.J. Nielsen, S.D. Pierce, and L. Washburn (2007), Delayed Upwelling Alters Nearshore Coastal Ocean Ecosystems in the Northern California Current, *PNAS, 104*(10) 3719-3724, doi:10.1073/pnas.0700462104.

Beaugrand, G., K.M. Brander, J.A. Lindley, S. Souissi, and P.C. Reid (2003), Plankton effect on cod recruitment in the North Sea, *Nature, 426*, 661-664, doi:10.1038/nature02164.

Botsford, L.W., C.A. Lawrence, E.P. Dever, A. Hastings, and J. Largier (2006), Effects of variable winds on biological productivity on continental shelves in coastal upwelling systems, *Deep-Sea Research II, 53*, 3116-3140, doi:10.1016/j.dsr2.2006.07.011.

Chavez, F.P., and M. Messie (2009), A comparison of Eastern Boundary Upwelling Ecosystems, *Progress on Oceanography, 83*, 80-96, doi:10.1016/j.pocean.2009.07.032.

Chhak, K., and E. Di Lorenzo (2007), Decadal variations in the California Current upwelling cells, *Geophys. Res. Lett., 34*, L14604, doi:10.1029/2007GL030203.

Collins, M. (2005), El Niño- or La Niña-like climate change?, *Climate Dynamics, 24*, 89-104, doi:10.1007/s00382-004-0478-x.

Di Lorenzo, E., N. Schneider, K.M. Cobb, P.J.S. Franks, K. Chhak, A.J. Miller, J.C. Williams, S.J. Bograd, H. Arango, E. Curchister, T.M. Powell, and P. Rivière (2008), North Pacific Gyre Oscillation links ocean climate to ecosystem change, *Geophys. Res. Lett., 35*, L08607, doi:10.1029/2007GL032838.

Edwards, M., and A.J. Richardson (2004), Impact of Climate Change on marine pelagic phenology and trophic mismatch, *Nature, 430*, 881-884, doi:10.1038/nature02808.

Garcia-Reyes, M., and J. Largier (2010), Observations of increased wind-driven coastal upwelling off central California, *J. Geophys. Res., 115*, C04011, doi:10.1029/2009JC005576.

Hales, B., T. Takahashi, and L. Bandstra (2005), Atmospheric CO2 uptake by a coastal upwelling system, *Global Biogeochemical Cycles, 19*, GB1009, doi:10.1029/2004GB002295.

Hickey, B.M., (1979), The California Current System – hypotheses and facts, *Prog. Oceanog., 8*, 191-279.

Hickey, B.M., and N.S. Banas (2008), Why is the North End of the California Current System so Productive?, *Oceanography, 21*(4) 90-107.

Hsieh, W.W., D.M. Ware, and R.E. Thomson (1995), Wind-induced upwelling along the west coast of North America, 1899-1988, *Can. J. Fish. Aquat. Sci., 52*, 325-244.

Ianson, D., and S.E. Allen (2002), A two-dimensional nitrogen and carbon flux model in a coastal upwelling region, *Global Biogeochemical Cycles, 16*(1), 1011, doi:10.1029/2001GB001451.

Ianson, D., R.A. Feely, C.L. Sabine, and L.W. Juranek (2009), Features of Coastal Upwelling Regions that Determine Net Air-Sea CO2 Flux, *Journal of Oceanography, 65*, 677-687.

Kalney, E., M. Kanamitsu, R. Kistler, W. Collins, D. Deaven, L. Gandin, M. Iredell, S. Saha, G. White, J. Woollen, Y. Zhu, M. Chelliah, W. Ebisuzaki, W. Higgins, J. Janowiak, K.C. Mo, C. Ropelewski, J. Wang, A. Leetmaa, R. Reynolds, R. Jenne, and D. Joseph (1996), The NCEP/NCAR 40-year reanalysis project, *Bull. Amer. Meteor. Soc., 77*, 437-470.

Lentz, S.J., and D.C. Chapman (2004), The Importance of Nonlinear Cross-Shelf Momentum Flux during Wind-Driven Coastal Upwelling, *Journal of Physical Oceanography, 34*, 2444-2457.

Lucas, A., and S. Jasson, Using amap and ctc Packages for Huge Clustering, *R News, 6*(5), 58-60.

Mackas, D.L. (2006), Interdisciplinary oceanography of the western North American continental margin: Vancouver Island to the tip of Baja California (8,E), pp. 441-502 in *The Sea*, Volume 14 ed. by A.R Robinson and K.H. Brink, Harvard University Press.

Mackas, D.L., R.E. Thomson, and M. Galbraith (2001), Changes in the zooplankton community of the British Columbia continental margin, 1985-1999, and their covariation with oceanographic conditions, *Can. J. Fish. Aquat. Sci., 58*, 685-702, doi:10.1139/cjfas-58-4-685.

Mantua, N.J., S.R. Hare, Y. Zhang, J.M. Wallace, and R.C. Francis (1997), A Pacific Interdecadal Climate Oscillation with Impacts on Salmon Production, *Bulletin of the American Meteorological Society, 78*(6), 1069-1079.

Merryfield, W.J., B. Pal and, M.G.G. Foreman (2009), Projected future changes in surface marine winds off the west coast of Canada, *J. Geophys. Res., 114*, C06008, doi:10.1029/2008JC005123.

Mesinger, F., G. DiMego, E. Kalnay, K. Mitchell, P.C. Shafran, W. Ebisuzaki, D. Jovic, J. Woollen, E. Rogers, E.H. Berbery, M.B. Ek., Y. Fan, R. Grumbine, W. Higgins, H. Li, Y. Lin, G. Manikin, D. Parrish, and W. Shi (2005), North American regional reanalysis, *Bulletin of the American Meteorological Society, 87*(3), 343-360, doi:10.1175/BAMS-87-3-343.

Moore, G.W.K., R.S. Pickart, and I.A. Renfrew (2008), Buoy observations from the windiest location in the world ocean, Cape Farewell, Greenland, *Geophys. Res Lett., 35*, L18802, doi:10.1029/2008GL034845.

Peterman, R.M., and B. Dorner (2012), A widespread decrease in productivity of sockeye salmon (Oncorhynchus nerka) populations in western North America, *Can. J. Fish. Aquat. Sci.*, *69*, 1255-1260, doi:10.1139/F2012-063.

Penland, C., D.-Z. Sun, A. Capotondi, and D. J. Vimont, 2010: A brief introduction to El Niño and La Niña. Chapter 3 in Climate Dynamics: Why does Climate Vary?, *Geoph. Monog. Series*, *189*, 53-64, doi:10.1029/2008GM000846.

Pond, S., and G.L. Pickard (1981), *Introductory dynamical oceanography*. Gulf Professional Publishing.

Pryor, S.C., R.J. Barthelmie, D.T. Young, E.S. Takle, R.W. Arritt, D. Flory, W.J., Gutowski Jr., A. Nunes, and J. Roads (2009), Wind speed trends over the contiguous United States, *J. Geophys. Res., 114*, D14105, doi:10.1029/2008JD011416.

R Core Team (2012), R: A Language and Environment for Statistical Computing, R Foundation for Statistical Computing, Vienna, Austria, ISBN 3-900051-07-0}, http://www.R-project.org.

Rasmusson, E.M., and J.M. Wallace (1983), Meteorological Aspects of the El Niño/Southern Oscillation, *Science, 222*(4629), 1195-1202.

Rodionov, S.N. (2004), A sequential algorithm for testing climate regime shifts, *Geophys. Res. Lett., 31*, L09204, doi:10.1029/2004GL019448.

Schwing, F.B., and R. Mendelssohn (1997), Increased coastal upwelling in the California Current System, *J. Geophys. Res., 102*(C2), 3421-3438.

Smith, R.L. (1994), The physical processes of coastal ocean upwelling systems in *Upwelling in the Ocean,* edited by C.P Summerhayes et al., pp. 39–64, Wiley, New York.

Snyder, M.A., L.C. Sloan, N.S. Diffenbaugh, and J.L. Bell (2003), Future climate change and upwelling in the California Current, *Geophys. Res. Lett., 30*(15), 1823, doi:10.1029/2003GL017647.

Thomson, R.E., and D.M. Ware (1996), A current velocity index of ocean variability, *J. Geophys. Res., 101*(C6) 14297-14310.

Tinis, S.W., R.E. Thomson, C.F. Mass, and B.M. Hickey (2006), Comparison of MM5 and Meteorological Buoy Winds from British Columbia to Northern California, *Atmosphere-Ocean, 44*(1), 65-81.

(Tortell, P.D., A. Merzouk, D. Ianson, R. Pawlowicz, and D. Yelland, Influence of regional climate forcing on surface water pCO2, ΔO2/Ar and dimethylsulfide (DMS) along the southern British Columbia coast, submitted to JGR 2012)

Trenbreth, K.E., W.G. Large, and J.G. Olsen (1990), The mean annual cycle in global ocean wind stress, *Journal of Physical Oceanography, 20*, 1742-1760.

Ware, D.M., and R.E. Thomson (1991), Link Between Long-Term Variability in Upwelling and Fish Production in the Northeast Pacific Ocean, *Can. J. Fish. Aquat. Sci, 48*, 2296-2306.

Ware, D.M., and R.E. Thomson (2005), Bottom-Up Ecosystem Trophic Dynamics Determine Fish Production in the Northeast Pacific, *Science, 308*, 1280-1284, doi:10.1126/science.1109049.

Winant, C.D., and J.R. Olsen (1976), The vertical structure of coastal currents, *Deep-Sea Research, 23,* 925-936.

Zoumakis, N.M. (1993), The dependence of the power-law exponent on surface roughness and stability in a neutrally and stably stratified surface boundary layer, Atmosfera, 6, 79-83.